Downloaded from https://www.science.org at Helmholtz Zentrum Mnchen - Zentralbibliothek on March 06, 2025

NEURODEVELOPMENTAL DISORDERS

PSMC3 proteasome subunit variants are associated with neurodevelopmental delay and type I interferon production

Frédéric Ebstein 1+, Sébastien Küry^{2,3+}, Victoria Most⁴, Cory Rosenfelt⁵, Marie-Pier Scott-Boyer⁶, Geeske M. van Woerden^{7,8,9}, Thomas Besnard^{2,3}, Jonas Johannes Papendorf¹, Maja Studencka-Turski¹, Tianyun Wang^{10,11,12}, Tzung-Chien Hsieh¹³, Richard Golnik¹⁴, Dustin Baldridge¹⁵, Cara Forster¹⁶, Charlotte de Konink^{7,8}, Selina M.W. Teurlings^{7,8}, Virginie Vignard^{2,3}, Richard H. van Jaarsveld¹⁷, Lesley Ades^{18,19}, Benjamin Cogné^{2,3}, Cyril Mignot^{20,21}, Wallid Deb^{2,3}, Marjolijn C.J. Jongmans^{17,22}, F. Sessions Cole¹⁵, Marie-José H. van den Boogaard¹⁷, Jennifer A. Wambach¹⁵, Daniel J. Wegner¹⁵, Sandra Yang¹⁶, Vickie Hannig²³, Jennifer Ann Brault²³, Neda Zadeh²⁴, Bruce Bennetts^{19,25}, Boris Keren²⁶, Anne-Claire Gélineau²⁶, Zöe Powis²⁷, Meghan Towne²⁷, Kristine Bachman²⁸, Andrea Seeley²⁸, Anita E. Beck²⁹, Jennifer Morrison³⁰, Rachel Westman³¹, Kelly Averill³², Theresa Brunet^{33,34}, Judith Haasters³⁵, Melissa T. Carter^{36,37}, Matthew Osmond³⁶, Patricia G. Wheeler³⁰, Francesca Forzano^{38,39}, Shehla Mohammed^{38,39}, Yannis Trakadis⁴⁰, Andrea Accogli⁴⁰, Rachel Harrison^{38,41}, Yiran Guo^{42,43}, Hakon Hakonarson⁴², Sophie Rondeau⁴⁴, Geneviève Baujat⁴⁴, Giulia Barcia⁴⁴, René Günther Feichtinger⁴⁵, Johannes Adalbert Mayr⁴⁵, Martin Preisel⁴⁵, Frédéric Laumonnier^{46,47}, Tilmann Kallinich^{48,49}, Alexej Knaus¹³, Bertrand Isidor^{2,3}, Peter Krawitz¹³, Uwe Völker⁵⁰, Elke Hammer⁵⁰, Arnaud Droit⁶, Evan E. Eichler^{10,51}, Ype Elgersma^{8,9}, Peter W. Hildebrand^{4,52,53}, François Bolduc^{5,54,55‡}, Elke Krüger^{1*‡},

A critical step in preserving protein homeostasis is the recognition, binding, unfolding, and translocation of protein substrates by six AAA-ATPase proteasome subunits (ATPase-associated with various cellular activities) termed PSMC1-6, which are required for degradation of proteins by 26S proteasomes. Here, we identified 15 de novo missense variants in the PSMC3 gene encoding the AAA-ATPase proteasome subunit PSMC3/Rpt5 in 23 unrelated heterozygous patients with an autosomal dominant form of neurodevelopmental delay and intellectual disability. Expression of PSMC3 variants in mouse neuronal cultures led to altered dendrite development, and deletion of the PSMC3 fly ortholog Rpt5 impaired reversal learning capabilities in fruit flies. Structural modeling as well as proteomic and transcriptomic analyses of T cells derived from patients with PSMC3 variants implicated the PSMC3 variants in proteasome dysfunction through disruption of substrate translocation, induction of proteotoxic stress, and alterations in proteins controlling developmental and innate immune programs. The proteostatic perturbations in T cells from patients with PSMC3 variants correlated with a dysregulation in type I interferon (IFN) signaling in these T cells, which could be blocked by inhibition of the intracellular stress sensor protein kinase R (PKR). These results suggest that proteotoxic stress activated PKR in patient-derived T cells, resulting in a type I IFN response. The potential relationship among proteosome dysfunction, type I IFN production, and neurodevelopment suggests new directions in our understanding of pathogenesis in some neurodevelopmental disorders.

Copyright © 2023 The Authors, some rights reserved; exclusive licensee American Association for the Advancement of Science. No claim to original U.S. Government Works

INTRODUCTION

Proteasomes are large multi-protein complexes whose structure is adapted to the function of regulated protein degradation, thereby controlling many cellular processes (1, 2). Together with the autophagosomal-lysosomal system, proteasomes maintain protein homeostasis by counterbalancing the synthesis of new proteins by the translational machinery (3-6). The proteasome is part of the ubiquitin-proteasome system (UPS), which counts numerous enzymes acting upstream of the proteasome (7, 8). Aged or unstructured proteins are preliminary ubiquitin-tagged by the ubiquitination machinery through a cascade of enzymatic reactions for degradation by the 26S proteasome (9, 10). The 26S proteasome

consists of two parts, the 20S core proteolytic particle and the 19S regulatory particle, which caps the 20S particle at one or both ends (11, 12). Polyubiquitinated proteins are recognized by the 19S regulatory particle, which comprises two parts: a base and a lid. In the base, four regulatory particle non-adenosine triphosphatase (ATPase) (Rpn) subunits (Rpn1, Rpn2, Rpn10, and Rpn13; encoded by the proteasome genes PSMD2, PSMD1, PSMD4, and ADRM1, respectively) ensure recognition and capture of ubiquitin-modified substrates (13, 14). The lid contains eight additional non-ATPase subunits, such as Rpn3, Rpn5-9, Rpn12, and Rpn15, which serve as scaffolds for binding of other subunits (15, 16) and the deubiquitinating enzyme Rpn11 (encoded by PSMD14)

(17). Six AAA-ATPase (ATPase-associated with various cellular activities) subunits (Rpt1 to 6), encoded by the genes PSMC1-6 in the base, use the energy provided by adenosine triphosphate (ATP) hydrolysis to unfold and translocate the substrate into the barrelshaped 20S proteolytic core particle by gate opening. The 20S complex comprises heptameric α - and β -rings with an $\alpha_{1-7}\beta_{1-7}\beta_{1-7}$ α_{1-7} architecture encoded by proteasome alpha subunit *PSMA1-7* or beta subunit genes *PSMB1-7*. The β -ring may be subjected to variations, thereby giving rise to two major proteasome isoforms, namely, standard and immunoproteasomes. Standard proteasomes typically contain the catalytic β 1, β 2, and β 5 subunits with caspase-, trypsin-, and chymotrypsin-like activities, respectively (18, 19). In immunoproteasomes, the \beta 1, \beta 2, and \beta 5 subunits are replaced by the inducible β 1i, β 2i, and β 5i subunits, encoded by the *PSMB9*, PSMB10, and PSMB8 genes, respectively (20). Although standard proteasomes are expressed in virtually all types of tissues, the expression of the inducible β subunits is restricted to immune cells and nonimmune cells exposed to type I or II interferons (IFNs) (21, 22).

Pathogenic variants in proteasome subunit genes cause rare proteasomopathies with a broad spectrum of symptoms (23, 24). So far, with the exception of the PSMB1 ($\beta 6$) subunit (25), all pathogenic variants related to the 20S core particle have been shown to provoke immune dysregulation. Several genes encoding β subunits (PSMB4, PSMB8, PSMB9, and PSMB10), α subunits (PSMA3), or assembly

chaperone genes [proteasome maturation protein (POMP) and proteasome assembly chaperone Pac2 gene (PSMG2)] of the 20S proteasome complex have been involved in autosomal recessive proteasome-associated autoinflammatory syndromes (PRAAS) typically characterized by persistent type I IFN signaling (26–33). By contrast, genetic disorders involving genes of the 19S regulatory particle such as the Stankiewicz-Isidor syndrome [STISS; Mendelian Inheritance in Man (MIM): 617516] caused by truncating variants of PSMD12 (also referred to as Rpn5) are neurodevelopmental polymalformative syndromes (34) with subclinical activation of type I IFN signaling (35, 36). These observations place both PRAAS and STISS in the category of type I interferonopathies, a recent family of genetically determined rare autoinflammatory syndromes with dysregulated type I IFN signaling that includes Aicardi-Goutières syndrome and familial chilblain lupus (37, 38). Clinically, these diseases are complex, demonstrating multiple organ involvement (often brain and skin), encompassing a broad range of phenotypes, and being associated with high morbidity and mortality (39). In this work, we identified 15 dominant de novo variants in the PSMC3 gene coding for the AAA-ATPase PSMC3/Rpt5. These rare missense variants were detected in 23 individuals presenting with neurodevelopmental delay (NDD), intellectual disability (ID), or both, together with various congenital malformations. Together, our data highlight interferonopathy as a potential contributor to the pathogenesis of NDD/ID in patients

¹Institut für Medizinische Biochemie und Molekularbiologie (IMBM), Universitätsmedizin Greifswald, Ferdinand-Sauerbruch-Straße, 17475 Greifswald, Germany. ²Nantes Université, CHU Nantes, Service de Génétique Médicale, 44000 Nantes, France. ³Nantes Université, CHU Nantes, CNRS, INSERM, l'institut du thorax, 44000 Nantes, France. ⁴Institut für Medizinische Physik und Biophysik, Universität Leipzig, Medizinische Fakultät, Härtelstr. 16-18, 04107 Leipzig, Germany. ⁵Department of Pediatrics, University of Alberta, Edmonton, AB CT6G 1C9, Canada. ⁶Research Center of Quebec CHU-Université Laval, Québec, QC PQ G1E6W2, Canada. ⁷Department of Neuroscience, Erasmus University Medical Center, 3015 CN, Rotterdam, Netherlands. *ENCORE Expertise Center for Neurodevelopmental Disorders, Erasmus University Medical Center, 3015 CN, Rotterdam, Netherlands. Department of Clinical Genetics, Erasmus University Medical Center, 3015 CN, Rotterdam, Netherlands. Department of Genome Sciences, University of Washington School of Medicine, Seattle, WA 98195, USA. ¹¹Department of Medical Genetics, Center for Medical Genetics, School of Basic Medical Sciences, Peking University Health Science Center, Beijing 100191, China. ¹²Neuroscience Research Institute, Peking University; Key Laboratory for Neuroscience, Ministry of Education of China & National Health Commission of China, Beijing 100191, China. ¹³Institute for Genomic Statistics and Bioinformatics, University Hospital Bonn, Rheinische Friedrich-Wilhelms-Universität Bonn, 53127 Bonn, Germany. ¹⁴Klinik für Pädiatrie I, Universitätsklinikum Halle (Saale), 06120 Halle (Saale), Germany. ¹⁵Edward Mallinckrodt Department of Pediatrics, Washington University School of Medicine, St. Louis, MO 63130-4899, USA. ¹⁶GeneDx, 207 Perry Parkway, Gaithersburg, MD 20877, USA. ¹⁷Department of Genetics, University Medical Center Utrecht, 3508 AB, Utrecht, Netherlands. ¹⁸Department of Clinical Genetics, Children's Hospital at Westmead, Locked Bag 4001, Westmead, NSW 2145, Australia. ¹⁹Disciplines of Genomic Medicine & Child and Adolescent Health, Faculty of Medicine and Health, University of Sydney, Sydney, NSW 2145, Australia. ²⁰APHP, Hôpital Pitié-Salpêtrière, Département de Génétique, Centre de Reference Déficience Intellectuelle de Causes Rares, GRC UPMC Déficience Intellectuelle et Autisme, 75013 Paris, France. ²¹Sorbonne Universités, Institut du Cerveau et de la Moelle épinière, ICM, Inserm U1127, CNRS UMR 7225, 75013, Paris, France. ²²Princess Máxima Center for Pediatric Oncology, 3584 CS Utrecht, Netherlands. ²³Department of Medicine, Vanderbilt University Medical Center, Nashville, TN 37232, USA. ²⁴Genetics Center and Division of Medical Genetics, Children's Hospital of Orange County, Orange, CA 92868, USA. ²⁵Sydney Genome Diagnostics, Western Sydney Genetics Program, Children's Hospital at Westmead, Sydney, NSW, 2145, Australia. ²⁶Département de Génétique, Centre de Référence des Déficiences Intellectuelles de Causes Rares, Groupe Hospitalier Pitié-Salpêtrière, Assistance Publique-Hôpitaux de Paris, 75013 Paris, France. ²⁷Departement of Clinical Research, Ambry Genetics, Aliso Viejo, CA 92656, USA. ²⁸Genomic Medicine Institute, Geisinger, Danville, PA 17822, USA. ²⁹Department of Pediatrics, Division of Genetic Medicine, University of Washington and Seattle Children's Hospital, Seattle, WA 98195-6320, USA. ³⁰Division of Genetics, Arnold Palmer Hospital for Children, Orlando Health, Orlando, FL 32806, USA. ³¹Division of Genetics, St. Luke's Clinic, Boise, ID 83712, USA. ³²Department of Pediatrics, Division of Pediatric Neurology, UT Health Science Center at San Antonio, San Antonio, TX 78229, USA. ³³Institute of Human Genetics, Technical University of Munich, School of Medicine, 81675 Munich, Germany. ³⁴Institute of Neurogenomics (ING), Helmholtz Zentrum München, German Research Center for Environmental Health, 85764 Neuherberg, Germany. ³⁵Klinikum der Universität München, Integriertes Sozialpädiatrisches Zentrum, 80337 Munich, Germany. ³⁶Children's Hospital of Eastern Ontario Research Institute, University of Ottawa, Otta Canada. ³⁷Department of Genetics, Children's Hospital of Eastern Ontario, Ottawa, ON K1H 8L1, Canada. ³⁸Wellcome Trust Sanger Institute, Wellcome Trust Genome Campus, Hinxton, Cambridge CB10 1SA, UK. ³⁹Clinical Genetics Department, Guy's and St Thomas' NHS Foundation Trust, London SE1 9RT, UK. ⁴⁰Division of Medical Genetics, McGill University Health Centre, Montreal, QC H4A 3J1, Canada. ⁴¹Department of Clinical Genetics, Nottingham University Hospitals NHS Trust, City Hospital Campus, the Gables, Gate 3, Hucknall Road, Nottingham NG5 1PB, UK. 42Center for Applied Genomics, Children's Hospital of Philadelphia, Philadelphia, Philadelphia, PA 19104, USA. ⁴³Center for Data Driven Discovery in Biomedicine, Children's Hospital of Philadelphia, Philadelphia, PA 19146, USA. ⁴⁴Service de Médecine Génomique des Maladies Rares, Hôpital Universitaire Necker-Enfants Malades, 75743 Paris, France. ⁴⁵University Children's Hospital, Salzburger Landeskliniken (SALK) and Paracelsus Medical University (PMU), 5020 Salzburg, Austria. ⁴⁶UMR 1253, iBrain, Université de Tours, Inserm, 37032 Tours, France. ⁴⁷Service de Génétique, Centre Hospitalier Régional Universitaire, 37032 Tours, France. ⁴⁸Department of Pediatric Respiratory Medicine, Immunology and Critical Care Medicine, Charité Universitätsmedizin Berlin, 13353 Berlin, Germany. ⁴⁹Deutsches Rheumaforschungszentrum, an institute of the Leibniz Association, Berlin and Berlin Institute of Health, 10117 Berlin, Germany. ⁵⁰Universitätsmedizin Greifswald, Interfakultäres Institut für Genetik und Funktionelle Genomforschung, Abteilung für Funktionelle Genomforschung, 17487 Greifswald, Germany. ⁵¹Howard Hughes Medical Institute, University of Washington, Seattle, WA 98195, USA. ⁵²Charité Universitätsmedizin Berlin, corporate member of Freie Universität Berlin and Humboldt-Universität zu Berlin, Institute of Medical Physics and Biophysics, Berlin, Germany. ⁵³Berlin Institute of Health, 10178 Berlin, Germany. ⁵⁴Neuroscience and Mental Health Institute, University of Alberta, Edmonton, AB T6G 2E1, Canada. ⁵⁵Department of Medical Genetics, University of Alberta, Edmonton, AB T6G 2H7, Canada.

^{*}Corresponding author. Email: elke.krueger@uni-greifswald.de (E.K.); stephane.bezieau@chu-nantes.fr (S.B.)

[†]The authors equally contributed to this work.

[‡]The authors equally contributed to this work.

carrying loss-of-function variants in subunits of the 19S proteasome regulatory particle and identify protein kinase R (PKR) as a major player in disease pathogenesis.

RESULTS

Identification of PSMC3 variants

The first *PSMC3* variant was detected in patient #2, a female newborn presenting with severe cardiac, gastrointestinal, inflammatory, and immune issues. Whole-exome sequencing (WES) highlighted the de novo nonsynonymous c.523A>G p.(M175V) variant (GenBank ID: NM_002804.4), which was absent in any public variant databases [Genome Aggregation Database (gnomAD, >246,000 chromosomes; NHLBI Exome Variant Server, >13,000 alleles; Bravo, 125,568 alleles] and predicted to be pathogenic by bioinformatics programs, including Sorting Intolerant from Tolerant (SIFT), PolyPHen-2n CADD, REVEL, and Metadome, as well as all programs compiled by MobiDetails (40). Our overall strategy described in Materials and Methods allowed us to identify a total of 15 distinct rare de novo missense *PSMC3* variants in 23 unrelated children presenting with a syndrome characterized by NDD and various congenital anomalies (Table 1).

As shown in Fig. 1, most of the *PSMC3* substitutions were localized in the AAA domain that was predicted to be intolerant to variations (fig. S1). Two distinct regions of the AAA domain were particularly prone to substitutions. The first hotspot was centered on the recurrent variant c.910C>T p.(R304W) detected in four unrelated children and encompassed variants c.910C>G p.(R304G),

c.915G>T p.(E305D), and c.929 T>C p.(M310T) (Fig. 1). The second region—enriched in rare variants [c.775A>G p.(M259V), c.776 T>C p.(M259T), c.782 T>C p.(I261T) (seen six times), c.784G>A p.(G262R), and c.806G>C p.(R269P)]—was more N-terminally located (Fig. 1). All 13 affected residues were highly conserved across species from mammalians down to fission yeast (Fig. 1). One major phenotypic hallmark of all individuals carrying PSMC3 variants was the predominance of neurodevelopmental or neuropsychiatric symptoms (table S1). In more detail, apart from patient #2, all affected children exhibited developmental delay (DD) (22 of 22; 100%) characterized by speech delay (19 of 19; 100%) alone or with ID (16 of 18; 89%) and motor delay (15 of 100%) alone or with 1D (16 of 18; 89%) and motor detay (15 of 19; 79%). Brain magnetic resonance imaging highlighted frequent anomalies (11 of 15; 73%), whereas the occurrence of abnormal behavior (9 of 18; 50%) and seizures (5 of 21; 24%) varied. Nine of 19 (47%) individuals experienced growth failure, most with feeding difficulties (8 of 18; 44%). Malformations were frequently observed in the skeleton [11 of 15; 73%; scoliosis, acetabular dysplasia, and brachymetatarsy), heart (10 of 18; 56%; ventricular or septal defects, patent ductus arteriosus, pulmonary hypertension, and atresia), kidney (4 of 15; 27%; horseshoe shape, pelvicalyceal dilatation, nephrocalcinosis, and multi-cystic dysplastic kidney), and head [microcephaly in 6 of 17 (35%); relative to severe macrocephaly in 2 of 16 (13%)]. Tumors were noted in 2 of 19 (11%) individuals (craniopharyngioma and neuroblastoma). Hearing loss was detected in 9 of 19 individuals (47%) and labeled as sensorineural in detected in 9 of 19 individuals (47%) and labeled as sensorineural in two and conductive in one of them, respectively. Most of the children (18 of 20; 90%) displayed dysmorphic facial features (fig. S2),

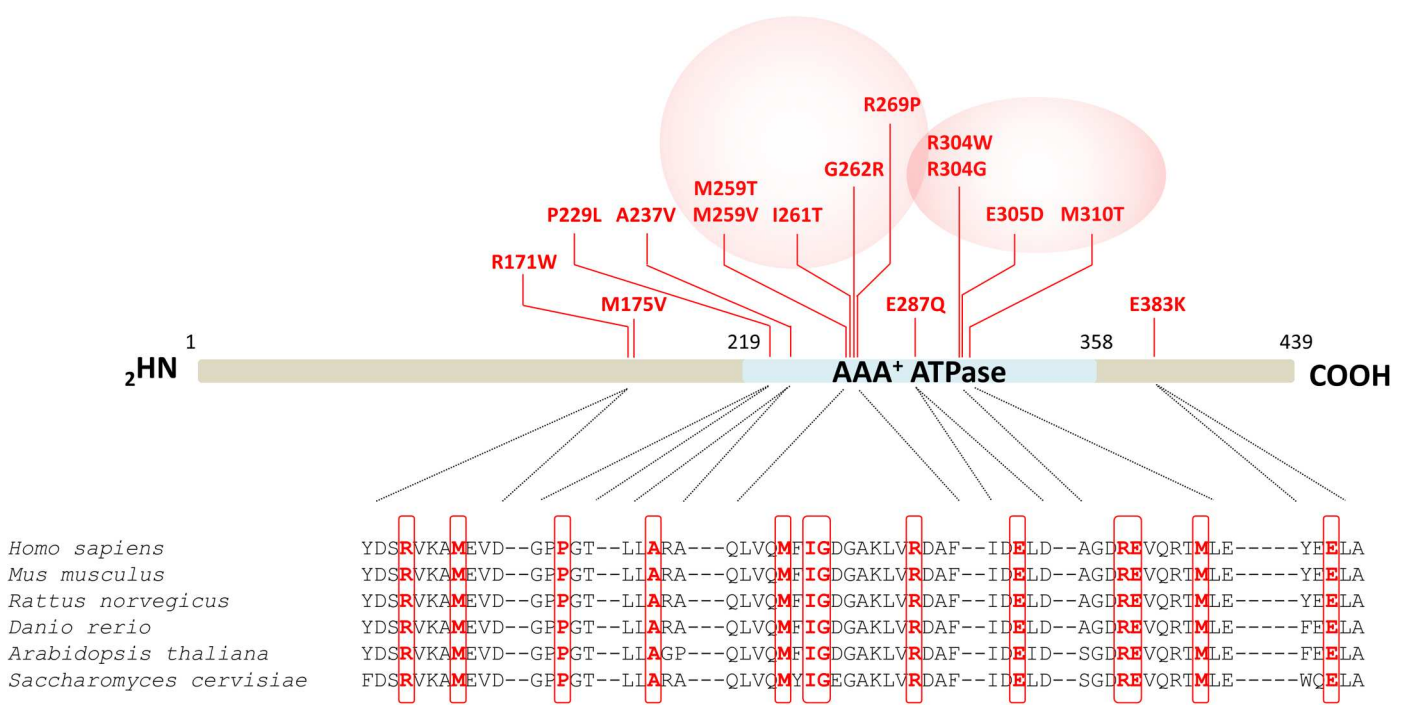


Fig. 1. Distribution of the de novo heterozygous PSMC3/Rpt5 variants identified in patients. Shown are the locations of the 15 NDD-causing missense variants (indicated in red) along the PSMC3/Rpt5 protein. The AAA-ATPase domain of the PSMC3/Rpt5 proteasome subunit of the 19S regulatory particle is depicted in blue. Pink circles indicate the presence of variants hotspots. A sequence alignment of regions immediately adjacent to the amino acids subjected to missense substitutions is also shown. Comparison of the PSMC3/Rpt5 primary structure across six eukaryotic organisms indicates the high conservation of the missense variant residues identified in patients with NDD/ID, which are highlighted by red boxes.

Table 1. Main characteristics of the *PSMC3* de novo variants* identified in the patients included in the study. ND, not determined; IFN, interferon; Metadome: I, intolerent; HI, highly intolerent; N, neutral.

Chromosomal localization (Chr11/ GRCh37)	cDNA change [†]	Protein change	Variant database‡	CADD Phred score (v1.6.)	Metadome	MobiDetails§	Effect on neuronal development	Effect on PSMC3 stability	Effect on proteasome assembly	Effect on mitophagy	IFN signature	Number of patients with the variant
g.47445677G>A	c.511C>T	R171W	rs775517283	27.3	1	45364	Improvement	Decrease	ND	ND	ND	1
g.47445665 T>C	c.523A>G	M175V	Absent	23.4	1	45365	ND	None	ND	ND	ND	1
g.47444430G>A	c.686C>T	P229L	Absent	25.5	l I	195979	ND	ND	ND	ND	ND	1
g.47444406G>A	c.710C>T	A237V	Absent	26.9	HI	45366	ND	Decrease	ND	ND	ND	1
g.47444234 T>C	c.775A>G	M259V	Absent	23.4	1	45367	ND	None	ND	ND	ND	1
g.47444233A>G	c.776 T>C	M259T	Absent	24.7	l I	45368	ND	Decrease	ND	ND	ND	1
g.47444227A>G	c.782 T>C	I261T	Absent	24.6	l I	45369	ND	Decrease	ND	ND	ND	6
g.47444225C>T	c.784G>A	G262R	Absent	26.8	I	45370	ND	None	None	Increase	Moderate	1
g.47444203C>G	c.806G>C	R269P	Absent	24	I	45371	ND	Decrease	ND			1
g.47444150C>G	c.859G>C	E287Q	Absent	26.7	I	45372	ND	Decrease	ND			1
g.47442253G>A	c.910C>T	R304W	rs1363348500	31	I	45373	Impairment	None	Impairment	Increase	Strong/ very strong	4
g.47442253G>C	c.910C>G	R304G	Absent	28.2	1	45374	ND	None	ND			1
g.47442248C>A	c.915G>T	E305D	Absent	23.1	1	45375	Impairment	None	Impairment	Increase	Moderate	1
g.47442234A>G	c.929 T>C	M310T	Absent	26.2	HI	45376	ND	None	ND			1
g.47440729C>T	c.1147G>A	E383K	Absent	27.8	N	45377	Impairment	None	ND			1

^{*}All variants presented are de novo, except variant c.775A>G, which is suspected de novo. † RefSeq transcript used for *PSMC3* is NM_002804.4. †gnomAD V3, dbSNP v154, ClinVar v20210828. §The access to detailed predictions for variant XXXXX (5364, 45365...) is as follows: https://mobidetails.iurc.montp.inserm.fr/MD/api/variant/XXXXX/browser/

including tall or broad forehead (7 of 19; 37%), thin upper lip with down-turned corners of mouth (6 of 19; 32%), abnormal palate (5 of 19; 265 of 19; 26%), epicanthal folds (5 of 19; 26%), and orofacial clefts (2 of 19; 10%). Computational analysis of facial morphology by GestaltMatcher (41) revealed that facial dysmorphism among the patients carrying *PSMC3* variants was rather heterogeneous, with similarities only observed between patients carrying identical variants (fig. S2).

Silencing of the *PSMC3 Drosophila* ortholog Rpt5 in adult flies fails to reverse stimulus contingencies

Given the neuronal nature of the phenotype of patients carrying *PSMC3* variants, we next sought to address the potential involvement of *PSMC3* in cognitive function by evaluating the learning performance of *Drosophila melanogaster* fruit flies with an RNA interference (RNAi) knockdown of Rpt5 (*Drosophila* ortholog of human *PSMC3*) expression by two different small interfering RNAs (siRNAs), namely, Rpt5³²⁴²² and Rpt5⁵³⁸⁸⁶ targeting Rpt5 transcripts at two different sites. To this end, we used a standard conditioning of odor-avoidance paradigm, in which animals were exposed to two different odors [3-octanol (OCT) or 4-methylcyclohexanol (MCH)], only one of which resulted in the simultaneous application of a foot shock (OCT⁺, MCH⁻), as previously described (Fig. 2, A and B) (42). Silencing of Rpt5 using Rpt5 RNAi under control of the neuron-specific embryonic lethal abnormal visual

system (Elav) promoter resulted in no substantial differences in learning performance for Rpt5 32422 [wild type (WT) versus Elav:RPT5 32422 , P=0.6435, n=4] or Rpt5 53886 [WT versus Elav:RPT5 53886 , P=0.5282, n=6] siRNAs (Fig. 2C). We next determined the reversal learning performance of Rpt5-silenced flies by training with an initial odor shock pairing (OCT $^+$, MCH $^-$) immediately followed by training with a reversed odor shock pairing (OCT $^-$, MCH $^+$) (Fig. 2B, bottom). Reversal learning performance was significantly poorer with pan-neuronal Rpt5 RNAi expression of Rpt5 32422 (WT versus Elav:RPT5 32422 , P<0.0001, n=4) or Rpt5 53886 (WT versus Elav:RPT5 53886 , P=0.0022, n=6) siRNAs. The three control groups once again did not significantly differ from each other (Fig. 2C). These data suggest that PSMC3 ortholog Rpt5 appears as a prerequisite for the changes in learned associations in D. melanogaster.

Ectopic expression of PSMC3/Rpt5 or its variants differentially affects neuronal development

In view of the negative impact of *PSMC3*/Rpt5 gene silencing on reversal learning, we next asked whether *PSMC3* was involved in the regulation of hippocampal neuron dendritic development. We therefore ectopically expressed WT PSMC3/Rpt5 in murine primary hippocampal neurons before neurite length quantification as previously described (*43*). As shown in fig. S3, expression of WT PSMC3/Rpt5 at an early developmental time point in vitro [day in

vitro (DIV) 3] resulted in significantly reduced neurite lengths of the neurons (empty vector versus PSMC3 WT, P = 0.0089). These results suggested that ectopic expression of WT PSMC3/Rpt5 may be detrimental to neurite outgrowth. We next sought to determine whether the different PSMC3/Rpt5 variants identified in patients with NDD/ID behaved differently compared with WT PSMC3/ Rpt5 in neurons when ectopically expressed. Expression of the R304W, E305D, and E383L PSMC3/Rpt5 variants resulted in similar neuronal morphological changes as those seen with WT PSMC3/Rpt5 (fig. S3). By contrast, expression of the M175V variant did not affect neuronal morphology when compared to the empty vector control and showed significant improvement when compared with WT PSMC3/Rpt5 (fig. S3). The positive effects exerted by the M175V PSMC3/Rpt5 variant on neurite length and arborization are intriguing but do not reflect an increased ability of the mutant subunit to incorporate into 19Scapped proteasome complexes (fig. S4). In addition, these observations do not preclude a milder pathogenicity of this variant, because the morphological changes seen are not necessarily beneficial for neurite outgrowth. Together, these results suggest that PSMC3/ Rpt5 participates in the regulation of neurite development and that any alteration of this gene might affect this process positively or negatively.

PSMC3 gene variants differentially affect PSMC3/Rpt5 steady-state protein expression

Because missense variants may cause haploinsufficiency by affecting mRNA and/or protein turnover, we next sought to determine the impact of the identified PSMC3 variants on PSMC3/Rpt5 steady-state protein expression. To this end, 13 of the PSMC3 variants were expressed in the SHSY5Y neuroblastoma cell line with a fused N-terminal hemagglutinin (HA) tandem repeat before Western blot analysis. As shown in Fig. 3A, the four PSMC3/Rpt5 variants carrying the R171W, A237V, M259V, and I261T mutations exhibited lower PSMC3/Rpt5 protein expression than their WT counterpart. Densitometric analysis of the HA-PSMC3 bands (Fig. 3A, bottom left) and of PSMC3 bands (Fig. 3A, bottom right) emerging from these constructs revealed that PSMC3/Rpt5 protein expression was reduced by about 90% when compared with WT HA-PSMC3 (Fig. 3A). However, all PSMC3 variants generated equivalent amounts of HA-PSMC3 transcripts in SHSY5Y cells in a 24-hour plasmid-driven expression, as determined by reverse transcription polymerase chain reaction (RT-PCR) and densitometric quantification (Fig. 3B), thereby indicating that reduced protein expression was due to increased protein turnover, decreased translation efficiency, or both. To determine whether these effects could be caused by nonpathogenic PSMC3 mutations as well, we next analyzed the steady-state expression of three HA-tagged single-nucleotide polymorphisms (SNPs) PSMC3/Rpt5 variants (I77N, I291V, and P355L) reported in the gnomAD. As shown in

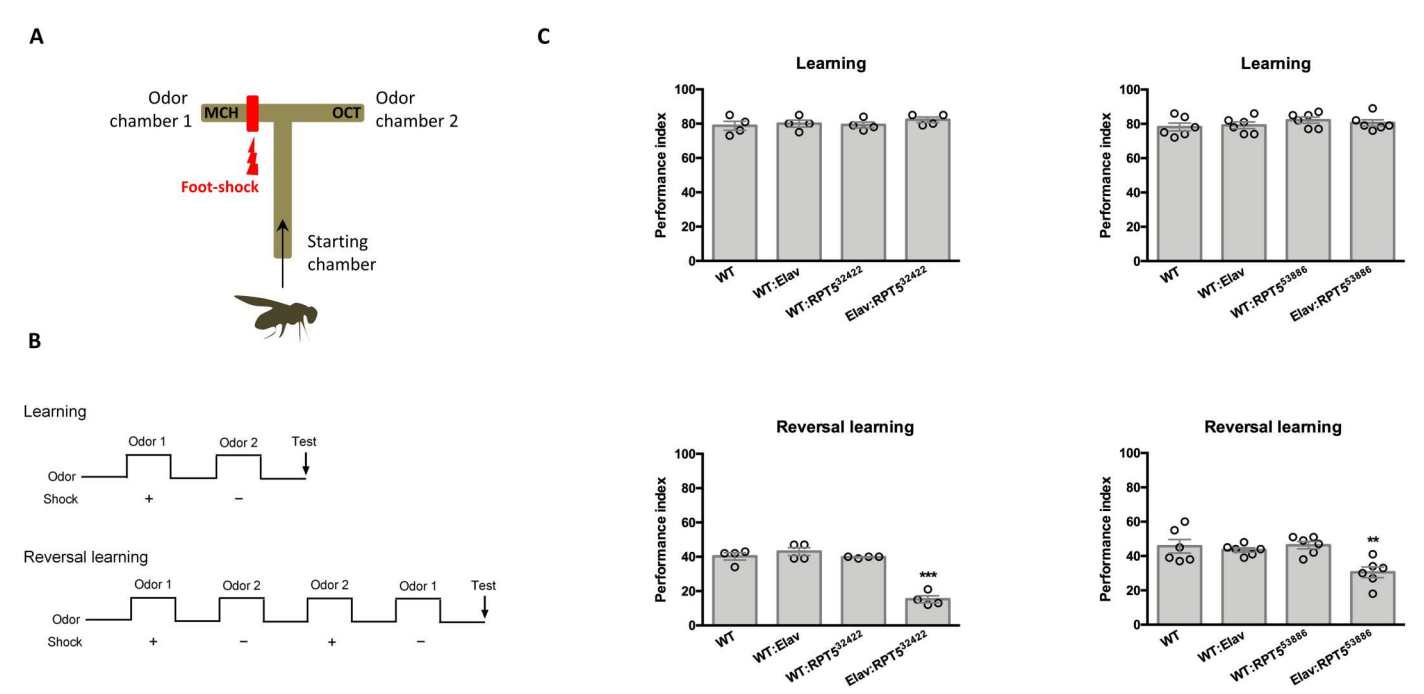


Fig. 2. Pan-neuronal RNAi-mediated knockdown of PSMC3/Rpt5 results in normal learning performance but defective reversal learning performance. (A) An illustration of a T-maze used for conditioning of odor avoidance in *Drosophila* is shown. Flies were trained to avoid one particular odor chamber that was associated with a foot shock (in this example, odor chamber 1). (B) Time course of the learning and reversal learning protocols used in these experiments is illustrated. Reversal learning was assessed by reversing odor shock pairing [4-methylcyclohexanol (MCH $^-$) and 3-octanol (OCT $^+$)], as indicated. (C) Top left: Learning performance index of wild-type (WT) flies, flies expressing Elav (WT:Elav), flies with full expression of Rpt5 32422 RNAi (Elav:Rpt5 32422 RNAi (WT:Rpt5 32422), and flies with pan-neuronal expression of Rpt5 53886 RNAi (Elav:Rpt5 53886), and flies with pan-neuronal expression of Rpt5 53886 RNAi (Elav:Rpt5 53886), and flies with pan-neuronal expression of Rpt5 53886 RNAi (Elav:Rpt5 53886) (P = 0.5282, P = 0.5282, P

fig. S5, the three investigated SNPs behaved similarly to their WT counterpart, suggesting that decreased PSMC3/Rpt5 protein expression may be a specific feature of some pathogenic variants.

Ectopic expression of HA-PSMC3/Rpt5 fusion proteins in SHSY5Y cells was accompanied by expression of untagged PSMC3/Rpt5 (Fig. 3A and fig. S5). One potential explanation for this observation implies a partial destruction of the HA epitope, as previously described (44). This assumption is, however, not supported by the fact that such a phenomenon was not observed when other proteasome AAA-ATPases such as PSMC5/Rpt6 were N-terminally tagged with the same HA epitope (fig. S6). Rather, it may be that the increased pools of untagged PSMC3/Rpt5 detected in cells expressing HA-PSMC3/Rpt5 might reflect a stabilization of endogenous PSMC3/Rpt5. Overexpressed and endogenous PSMC3/Rpt5 proteins might undergo self-association, resulting in the formation of homomers protecting them from degradation. To address this point, HA-PSMC3/Rpt5 fusion proteins were pulled down from SHSY5Y cells using HA antibody followed by Western blot analysis for PSMC3/Rpt5. As shown in fig. S7, HA-PSMC3 coprecipitated with untagged PSMC3/Rpt5, thereby confirming physical interaction between overexpressed and endogenous PSMC3/Rpt5. However, although the regulation of the PSMC3/Rpt5 subunit in response to concentration changes is potentially interesting, the observation that this feature does not vary between WT and stable PSMC3 variants suggests that this is not relevant to disease pathogenesis. Together, these data showed that the PSMC3 missense variants identified in patients with NDD/ID differentially affect protein expression and stability.

Structural modeling predicts that PSMC3 substitutions affect inter- and intramolecular interactions between proteasome subunits

We next attempted to predict the structural consequences of each of the 14 PSMC3 substitutions by assessing the localization of the mutated residues in the human 26S proteasome structure generated by Dong et al. (45) [Protein Data Bank (PDB) entry code: 6MSK]. Most of the affected amino acids emerged within the N-terminal α / β domain of PSMC3/Rpt5 with five residues (G262, I261, M259, R304, and E305) residing in two loops adjacent to the substrate tunnel pointing toward the center of the AAA-ATPase ring (Fig. 3, C and D). Specifically, on one loop, G262 was fixed by a main chain hydrogen bond to E305, thereby promoting flexibility of the preceding loop containing M259. Besides, E305 itself was held through a salt bridge by R308, with its preceding residue R304 involved in a polar network stabilizing the neighboring loop (fig. S8). Because these six residues stabilized or were part of the tertiary structure of the loops, any alteration of these amino acids is predicted to affect substrate trafficking and interactions with other AAA-ATPase subunits. As shown in fig. S8, the A237V variant was more difficult to classify and did not reveal itself structurally at first sight. However, one cannot exclude that the slight increase in residue size at position 237 might lead to structural changes. The overexpression assays in SHSY5Y cells suggest that such substitution does affect side chain packing and protein stability (Fig. 3A). The E383L missense variant was the only substitution lying within the C-terminal α-helical domain of PSMC3/Rpt5 adjacent to the 19S-20S interface. E383 held Q166 from the PSMA1/α6 subunit for polar interactions with both of the R169 and R386 residues (Fig. 3E). Changing the negatively charged E383 to a

positively charged K383 is therefore predicted to disrupt such a hydrogen bond network and affect the association of the 19S complex with the 20S core particle. E287 was also located in close proximity to the ATP binding site (fig. S8), and its substitution with Q287 presumably generated additional polar bonds with N333 likely to affect ATP binding, hydrolysis, or both. R171 was positioned at the PSMC3/Rpt5-PSMC2/Rpt1 interface and was part of a polar network involving the neighboring D169 and Q258 residues (fig. S9). As such, the substitution of positively charged arginine to hydrophobic tryptophan at this position is predicted to disrupt these interactions and a fortiori to affect the contact between the two subunits (fig. S9). The change of M175to V175 resulted in the loss of a polarized thiol group and hydrophilic environment, which was likely to destabilize the tertiary structure of this protein region (fig. S9). Together, these data suggest that the complex 26S proteasome structure may be strongly affected by the identified *PSMC3* missense variants, although an incorporation of the dysfunctional PSMC3/Rpt5 subunit with no detrimental effects of proteasome structure cannot be fully excluded. **PSMC3 variants differentially affect proteasome assembly**To further address the pathogenicity of the *PSMC3* variants, T cells from patients #13, #18, and #21 were analyzed for their proteasome contents. The intracellular expression of the α7 proteasome subunits and PA28-α did not vary between relative controls (father, mother, or both) and index cases (Fig. 4A). Likewise, the abundance

mother, or both) and index cases (Fig. 4A). Likewise, the abundance of the 19S subunit PSMD12/Rpn5 in mutant T cells was comparable to that detected in their control counterparts. T cells expanded from controls and patients exhibited two prominent PSMC3/Rpt5 immunoreactive bands migrating at about 50 and 40 kDa (Fig. 4A). Although the upper band running at ~50 kDa corresponded to the PSMC3/Rpt5 expected size, the nature of the lower band running at ~40 kDa was unclear. It is, however, unlikely that this band may be nonspecific, because it was detectable in T cells using another anti-PSMC3/Rpt5 antibody or in other cell types (fig. S10). This additional species might reflect a shorter, as-yet-undescribed PSMC3/Rpt5 isoform or a processed form arising from the PSMC3/Rpt5 full-length protein. Nevertheless, the unchanged protein expression profile of PSMC3/Rpt5 between controls and patients indicates that none of these phenomena is affected by any of the PSMC3 variants. Likewise, none of PSMC3 variant T cells showed reduced expression of the PSMC3/Rpt5 full-length protein, suggesting that proteasome dysfunction in these affected individuals was not caused by haploinsufficiency.

Next, T cells from affected individuals and relative controls were analyzed for proteasome complex formation and activity by in-gel fluorescence followed by Western blotting on native polyacrylamide gel electrophoresis (PAGE). As shown in Fig. 4B, the chymotrypsinlike activity of the 26S and 20S proteasome complexes [fluorogenic peptide-aminomethyl coumarin (LLVY-AMC)] was reduced for the majority of comparisons between patients and controls. Subsequent Western blot analysis revealed that the decreased 20S activity observed in patient #21 was associated with a decreased pool of 20S-PA28 complexes, as determined by reduced band intensity for the α6 and PA28 proteins. The amounts of unbound PA28-α/β complexes in T cells were increased in patient #13 and decreased in patient #18 (Fig. 4B). The reasons for these contrasting data between these two patients are unclear but might reflect distinct abilities to compensate for proteasome dysfunction. It should be

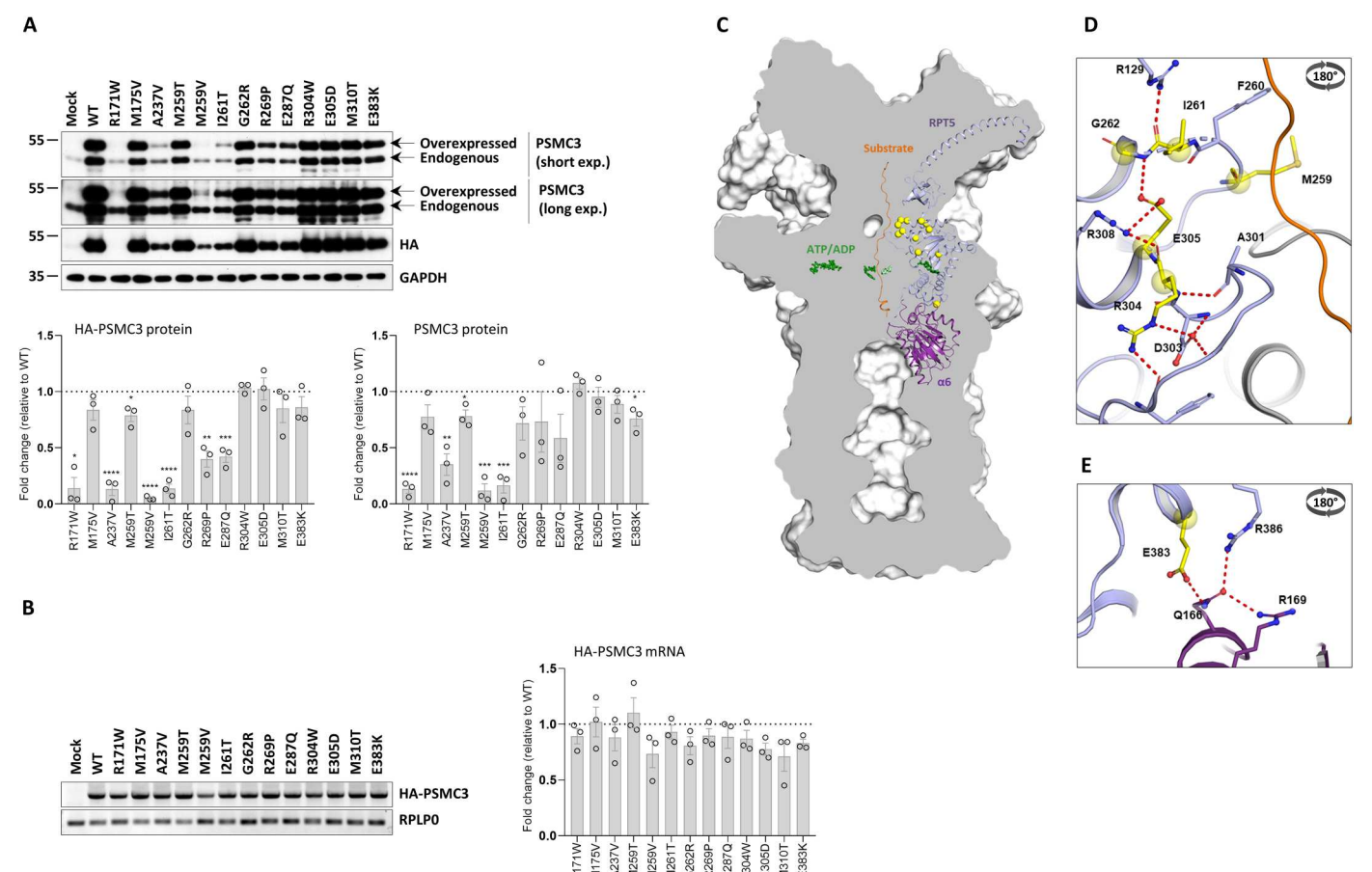


Fig. 3. PSMC3/Rpt5 protein variants do not behave similarly at the molecular level. (A) Top: SHSY5Y cells were transfected with HA-tagged PSMC3 mutants for 24 hours before protein extraction and Western blotting using antibodies specific for PSMC3/Rpt5 and HA, as indicated. Nontransfected and mock-transfected cells served as negative controls. Equal protein loading was ensured by probing the membranes with an anti-\alpha-tubulin monoclonal antibody (two exposure times are shown). Arrows indicate overexpressed and endogenous PSMC3/Rpt5. One representative experiment of three is shown. Bottom: Quantification of HA-tagged and untagged PSMC3/Rpt5 proteins in transfected SHSY5Y cells by densitometry. Data are presented as protein fold changes to WT PSMC3/Rpt5 proteins whose densitometry measurements were set to 1 (grid line) after normalization with GAPDH. Mean values ± SEM from three independent experiments are shown. Statistical significance was assessed by unpaired Student's t test (*P < 0.05, **P < 0.01, ***P < 0.001, and ****P < 0.0001). (B) Left: SHSY5Y cells that were transfected with HA-PSMC3 variants were subjected to total RNA extraction followed by semi-quantitative PCR using primer located in PSMC3 and the bovine growth hormone (BGH) polyadenylation signal of the pcDNA3.1/myc-HIS expression vector. Equal loading between the samples was ensured by amplifying the RPLO gene, as indicated. Right: Quantification of HA-tagged PSMC3 transcripts in transfected SHSY5Y cells by densitometry. Data are presented as mRNA fold changes to WT HA-PSMC3 mRNA whose densitometry measurements were set to 1 (grid line) after normalization with RPLPO. Mean values ± SEM from three independent experiments are shown. (C) A sliced surface view of the 26S proteasome (gray) was superimposed with a cartoon representation of the subunit PSMC3/RPT5 (blue) and PSMB1/ α 6 (purple) as well as the substrate (orange). The ATP/adenosine diphosphate (ADP) molecules of the AAA-ATPase ring are shown as green sticks, whereas the positions of the investigated missense variants are indicated as bright yellow spheres. (D) Detailed representation of the missense variants in the loop region of the N-terminal α/β domain. The residues affected by these variants are involved in a polar interaction network close to the substrate tunnel (view rotated by 180° around the x axis). (E) Close-up view on the RPT5-a6 interface affected by the E383L variant. Residues affected by this variant are shown as bright yellow balls and sticks with atoms colored by polarity (oxygen in red, nitrogen in blue, and sulfur in dark yellow; view rotated by 180° around the x axis).

noted, however, that, in contrast to PA28-bound proteasomes whose amounts did not change in these patients, free PA28- α/β are not equipped with protease activity and as such have no impact on intracellular proteolysis. Densitometric analysis of the PSMC3/Rpt5 signals revealed impaired subunit incorporation into 26S, hybrid and 30S proteasome complexes in patients when compared with controls (P = 0.0329) (Fig. 4B, bottom). Diminished expression of the α 6 and PSMC3/Rpt5 subunits was observed in the 26S proteasomes of patient #18 (Fig. 4B), indicating that the decline in 26S activity detected in this patient was likely to be attributed to

decreased amounts of 26S complexes. Likewise, the PSMC3/Rpt5 contents in 26S complexes were also reduced in patient #21 (Fig. 4B). Unexpectedly, 20S and 26S proteasome pools of patient #13 did not substantially vary when compared with those of the related control (Fig. 4B). The minor effects exerted by the G262R substitution in patient #13 may be partially explained by the fact that G262 is surrounded by a large amount of empty space (fig. S11), thereby allowing this region of the PSMC3/Rpt5 protein to accommodate mutations to some extent. Nevertheless, these data indicated that both of the R304W and E305D PSMC3/Rpt5 variants

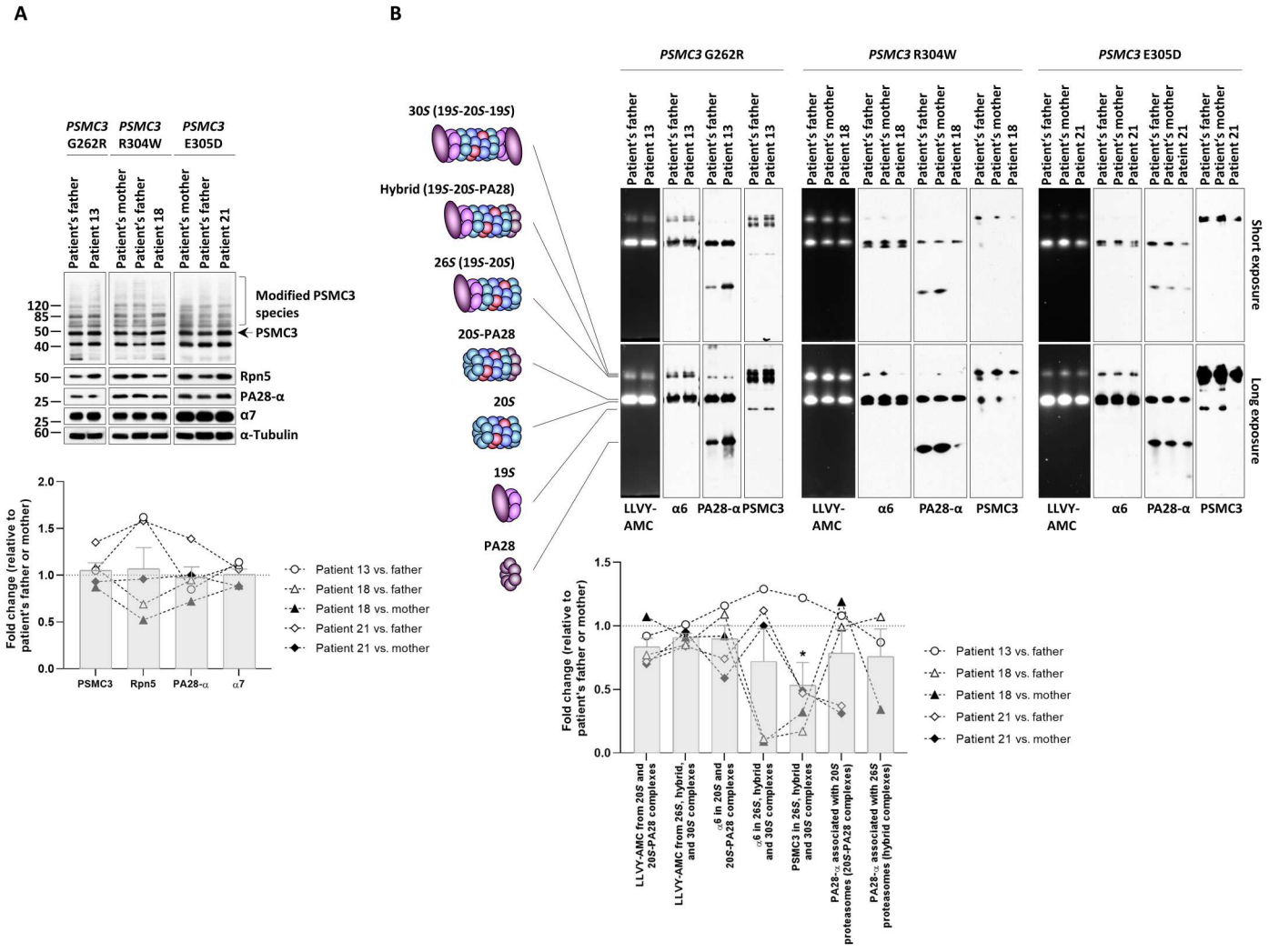


Fig. 4. PSMC3/Rpt5 protein variants lead to proteasome assembly defects in patient T cells. (A) Top: Five to 20 μg of radioimmunoprecipitation assay (RIPA) lysates from T cells isolated from patients #13, #18, and #21 and related controls (index case's father and/or mother) were separated by SDS-PAGE, followed by Western blotting using antibodies directed against PSMC3/Rpt5, PSMD12/Rpn5, PA28-α, and α7, as indicated. Equal protein loading was ensured by probing the membrane with an anti–α-tubulin antibody. Arrow indicates full-length PSMC3/Rpt5 migrating at the predicted size of about 50 kDa. High–molecular weight (HMW)–modified PSMC3/Rpt5 species are marked by a bracket. Bottom: Quantification of the Western blots by densitometry. Data are presented as fold changes in patients #13, #18, and #21 versus their father, mother, or both, whose densitometric measurements were set to 1 (grid line), as indicated. Columns indicate the fold change mean values ± SEM calculated from the five normalizations. (**B**) Top: Twenty micrograms of T cell lysates from patients #13, #18, and #21 and their parents (mother and/or father) were separated by 3 to 12% native PAGE. Proteasome chymotrypsin-like activity was assessed in gels using the LLVY-AMC fluorogenic peptide, as indicated. Gels were subsequently subjected to Western blotting using antibodies specific for α6, PSMC3/Rpt5 and PA28-α, as indicated. The schematic to the left depicts the proteasome complexes (305, hybrid, 265, 205-PA28, and 205) and free regulators (195 and PA28) detected by the three antibodies. Bottom: Quantification of the LLVY-AMC fluorescent signals and α6, PA28-α, and PSMC3 immunoreactive bands in 205 (short exposure), 205-PA28 (short exposure), 265 (long exposure), hybrid (long exposure), and/or 305 (long exposure) proteasome complexes by densitometry, as indicated. Data are presented as activity (LLVY-AMC) and protein (α6, PA28-α, and PSMC3) fold changes in patients #13, #18, and #21 versus their father and/or mother, whose densitometric measuremen

affect 20S proteasome assembly, 26S proteasome assembly, or both in individuals with NDD/ID, whereas the G262R variant has little impact in this process (Table 1).

Quantitative proteomics identifies cellular pathways affected by *PSMC3* loss of function in patients with NDD/ID

To better understand the cellular consequences of PSMC3 loss of function, we next performed a mass spectrometry-based

comparative analysis of the T cell proteomes of patient #17 and patient #21 (R304W and E305D, respectively) with that of their relative controls. As shown in Fig. 5, our data identified a protein signature consisting of 17 ribosomal proteins of the small 40S (RPS) or large 60S (RPL) ribosomal subunits that were specifically up-regulated in both investigated patients. This suggests that mRNA translation is a major affected pathway upon *PSMC3* loss of function, a notion that is further supported by the fact that components of the

mRNA processing machinery such as CUG-binding protein Elavlike family member 1 (CELF1), a member of the LSm family of RNA binding proteins (LSM1), RNA polymerase II CTD phosphatase (SSU72), and inosine triphosphatase were also differentially expressed between patients and controls (Fig. 5). Other notable proteins whose abundances varied in patients carrying PSMC3 variants included components of the immune system such as MX dynamin-like GTPase 1 (MX1), a typical IFN-stimulated gene (ISG) product, and the α chain of the IL3 receptor (IL3RA). These proteins were regulated in opposite directions, with both patients exhibiting higher amounts of MX1 but reduced amounts of IL3RA (Fig. 5). Our analysis further revealed that PSMC3 loss of function was also associated with increased protein expression of the H1.5 and H1.2 linker histone H1 variants, a finding that is in line with a role of the UPS in chromatin regulation (46). Protein set enrichment analysis uncovered that most of the significant (P < 0.05) proteomic changes between control and patients carrying PSMC3 variants were related to mRNA metabolism and translation (fig. S12), confirming that protein synthesis was dysregulated in these patients. Other differentially expressed proteins found to be enriched in T cells with PSMC3 variants belonged to the category of viral processes (fig. S12), unveiling a potential relationship between proteasome loss of function and innate immunity. Collectively, these data suggested that patients with PSMC3 variants exhibit alterations in basic cellular processes, including mRNA translation, immune signaling, and chromatin remodeling.

PSMC3 variants cause proteotoxic stress in T cells from patients

Proteasome dysfunction has been shown to be accompanied by accumulation of ubiquitin-protein conjugates and proteotoxic stress (24). As shown in Fig. 6A, all four investigated patients exhibited typical features of unbalanced protein homeostasis, as evidenced by the increased accumulation of ubiquitin-modified species when compared with their respective related controls using immunoblotting and densitometric analysis. Proteotoxic stress is known to induce the unfolded protein response and integrated stress response (UPR and ISR, respectively) (24, 47). To address this point, we quantified the expression of the glucose-regulated protein 94 chaperone protein [GRP94; the heat shock protein 90 kDa in the endoplasmic reticulum (ER)], whose up-regulation is understood to be a major hallmark of the UPR (48). The expression of GRP94 was increased in all patients (Fig. 6A). However, the activation of the UPR was only partial, because the phosphorylation and activation status of two other UPR markers, namely, serine/ threonine-protein kinase/endoribonuclease inositol-requiring enzyme 1 α (IRE1) and eukaryotic translation initiation factor 2 (eIF2)α, were not changed between controls and patients carrying PSMC3 variants (Fig. 6A). The failure to detect increased phosphorylated eIF2a, although the upstream kinase PKR was consistently activated in all patients (Fig. 6A), can be explained by up-regulation of both eIF2a phosphatases GADD34 (growth arrest and DNA damage-inducible protein 34) and CReP (constitutive repressor of eIF2α phosphorylation) across all four patients. Immunoblotting and densitometric analysis revealed that T cells of the patients carrying PSMC3 variants were also endowed with increased protein expression of microtubule-associated protein 1A/1B light chain 3 phosphatidylethanolamine conjugate LC3b-II (Fig. 6B), suggesting that the inability of these cells to eliminate ubiquitin-protein

aggregates cells via their 26S proteasomes triggers a compensatory mechanism mediated by activation of the autophagy system. Consistently, the mitochondrial proteins PINK1 (PTEN-induced putative kinase protein 1) and Bnip3L/NIX (BCL2/adenovirus E1B 19kDa protein-interacting protein 3-like/NIP3-like protein X) were found to be decreased in the patients carrying PSMC3 variants (Fig. 6B and Table 1), supporting the notion that selective autophagic processes, including mitophagy, were activated upon PSMC3 disruption. Because proteasome impairment typically results in the release of the TCF11/Nrf1 (transcription factor 11/nuclear factor erythroid-derived 2 like 1) protein from the ER membrane (49, 50), we next sought to determine the TCF11/Nrf1-processing pattern in NDD/ID-affected individuals. However, no differences in the TCF11/Nrf1-processing pattern could be detected between controls and patients carrying PSMC3 variants (Fig. 6B), suggesting that PSMC3 variants associated with NDD/ID do not lead to activation of the TCF11/Nrf1 signaling pathway.

T cells from patients with *PSMC3* variants exhibit a type I IFN signature

Because proteasome loss of function results in the generation of a typical type I IFN response in patients with PRAAS (30), we next sought to determine whether alterations in the PSMC3 gene would induce type I IFN signatures as well. To this end, we undertook a comparative examination of the mRNA expression of 750 predefined immunologically relevant genes in T cells from patients carrying PSMC3 variants and relative controls (father and/or mother) using the NanoString nCounter platform. A total of 30 differentially expressed genes could be identified, including 11 ISGs that were specifically up-regulated in all patients carrying PSMC3 variants (Fig. 7A), suggesting that PSMC3 loss of function is associated with type I IFN responses. The transcriptomic analysis of control and patient T cells further revealed that *PSMC3* disruption resulted in the up-regulation of genes of the notch signaling pathway such as NOTCH2 (neurogenic locus notch homolog protein 2) and JAG2 (protein jagged-2) involved in developmental pathways, including neurodevelopment (Fig. 7A) (51). To validate the type I IFN gene signature revealed by our omics profiling, we next evaluated the expression of seven ISGs (IFI27, IFI44L, IFIT1, ISG15, MX1, RSAD2, and IFI44) in samples of these four families with PSMC3 missense variants. As shown in Fig. 7B, all four affected children's samples (patients #13, #17, #18, and #21) exhibited much higher ISG expression than their parents (father and/or mother; Table 1). Calculation of the fold change median of the seven ISGs revealed that a significant increase was detected in all PSMC3 index cases when compared with their respective controls (patient #13 versus father, P = 0.0148; patient #17 versus mother, P = 0.0008; patient #18 versus father, P = 0.0002, patient #18 versus mother, P = 0.0011; patient #21 versus father, P = 0.0012; and patient #21 versus mother, P = 0.0142) (Fig. 7B). The strongest type I IFN signature was observed in patient #18, whose ISGs were up-regulated by approximately 40- or 10-fold when compared with the father or mother, respectively. Patients #13, #17, and #21 exhibited a milder type I IFN induction characterized by a two- to sixfold increase in ISG transcripts compared with their respective controls. Among the seven ISGs tested, IFIT1 and IFI44L were the genes that underwent the most pronounced up-regulation in all four affected individuals.

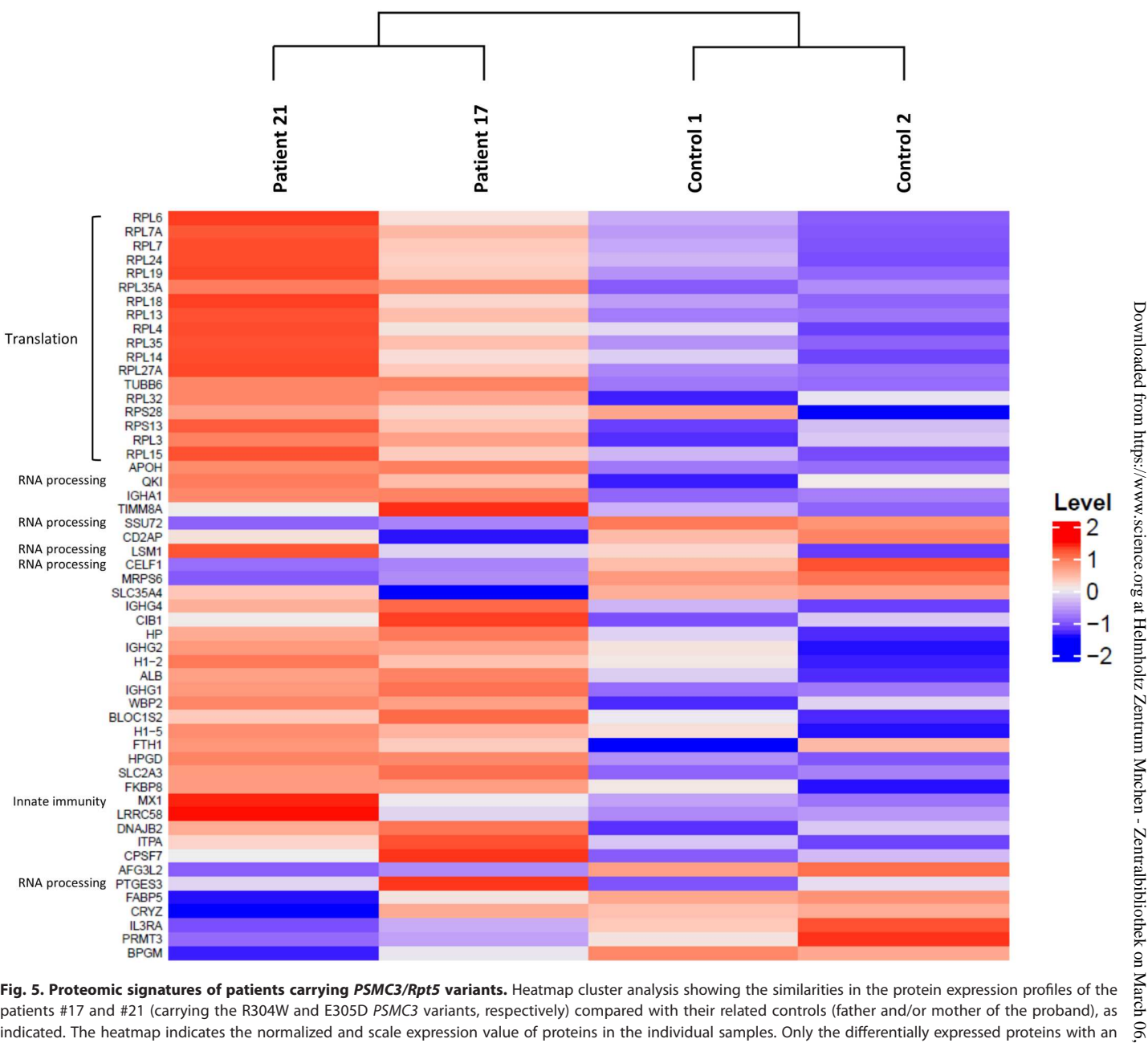


Fig. 5. Proteomic signatures of patients carrying PSMC3/Rpt5 variants. Heatmap cluster analysis showing the similarities in the protein expression profiles of the patients #17 and #21 (carrying the R304W and E305D PSMC3 variants, respectively) compared with their related controls (father and/or mother of the proband), as indicated. The heatmap indicates the normalized and scale expression value of proteins in the individual samples. Only the differentially expressed proteins with an absolute value of log₂ fold change greater than 2 were selected for the clustering analysis.

The type I IFN signature in T cells from patients with PSMC3 variants is PKR dependent

We next calculated and compared the IFN scores of both patients carrying *PSMC3* variants and their related controls with those of T cells isolated from six healthy donors. As shown in Fig. 8A, three of the related controls had an IFN score slightly above the cut-off value of 2.466 defined by Rice et al. (52) to be abnormal. However, the IFN scores of all related and unrelated controls remained significantly lower than those of the four tested patients (P = 0.0845and P = 0.0044), thereby confirming that these PSMC3 variants were associated with enhanced type I IFN signaling. A second independent assessment of patient #18 at 14 months after enrollment

revealed that this patient still exhibited a very high type I IFN score (fig. S13). Because all three inducible immunoproteasome subunits-β1i (PSMB9), β2i (PSMB10), and β5i (PSMB8)-are encoded by genes typically stimulated by type I and II IFN (20), we next asked whether PSMC3 loss of function was accompanied by a switch from standard proteasomes to immunoproteasomes. As illustrated in fig. S14, the steady-state expression of these subunits in T cells did not substantially change between control and patients, as determined by Western blotting. This may be because T cells, as immune cells, express high amounts of immunoproteasomes, a feature that renders any further protein up-regulation of the inducible subunits very difficult (53).

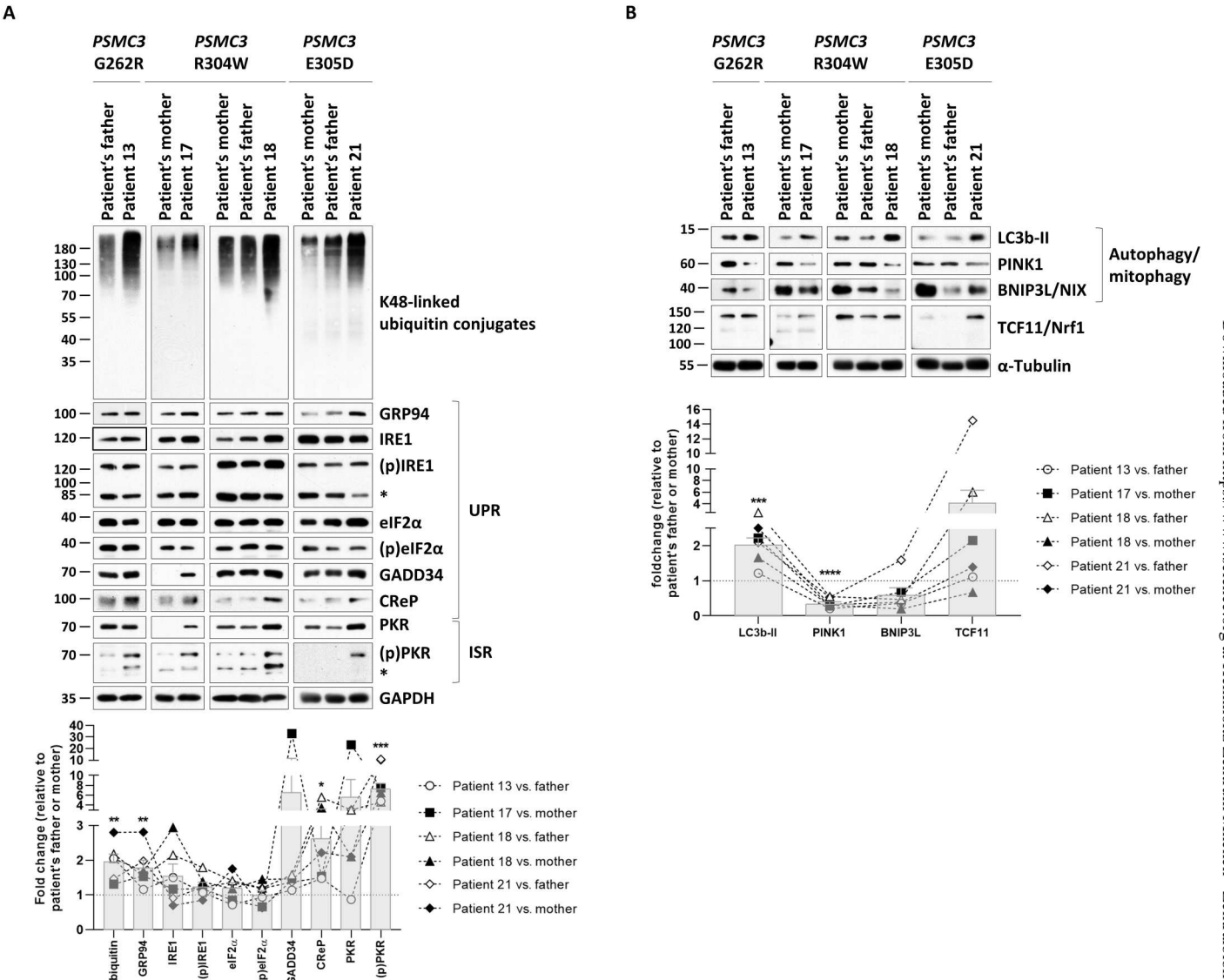


Fig. 6. T cells from patients with *PSMC3/Rpt5* missense variants exhibit signs of protein homeostasis perturbations and alterations of the UPR, ISR, and autophagy/mitophagy pathways. (A) Top: Five to 20 μ g of RIPA lysates from T cells isolated from patients #13, #17, #18, and #21 and related controls (*PSMC3* index case's father and/or mother) were separated by SDS-PAGE followed by Western blotting using antibodies directed against K48-linked ubiquitin-modified proteins, such as GRP94, IRE1, phospho-IRE1, eIF2 α , phospho-eIF2 α , GADD34, CReP, PKR, phospho-PKR, and GAPDH (loading control), as indicated. Bottom: Quantification of the Western blots by densitometry is shown. Data are presented as fold changes in patients #13, #17, #18, and #21 versus their father and/or mother, whose densitometric measurements were set to 1 (grid line), as indicated. Columns indicate the fold change mean values \pm SEM calculated from the six normalizations. Statistical significance was assessed by unpaired Student's test (*P < 0.05, **P < 0.01, and ****P < 0.001). (B) Top: RIPA cell lysates from patients #13, #17, #18, and #21 and their related controls (index case's father and/or mother) were subjected to SDS-PAGE/Western blotting using antibodies specific for LC3b-II, PINK1, BNIP3L, and α -tubulin (loading control), as indicated. Bottom: Quantification of the Western blots by densitometry. Data are presented as protein fold changes in patients #13, #17, #18, and #21 versus their father and/or mother, whose densitometric measurements were set to 1 (grid line), as indicated. Columns indicate the fold change mean values \pm SEM of the six normalizations. Statistical significance was assessed by unpaired Student's test (***P < 0.001 and ****P < 0.0001).

We next attempted to unravel the mechanisms by which type I IFN responses were initiated in patients carrying *PSMC3* loss-of-function variants. Having shown that all four affected patients exhibited marked alterations in the mitophagy, UPR, and ISR pathways (Fig. 6), we postulated that the dysregulation of either one of these pathways might act as a danger signal triggering innate immunity. To address this point, we inhibited key players of the UPR and/ or ISR, including PKR, IRE1, and GADD34 (24), by treating

patients' T cells with the C16, 4µ8C, or Guanabenz inhibitors, respectively. In addition, the potential implication of mitophagy-mediated mitochondrial DNA in this process was investigated by treating the cells with H-151, an inhibitor of the cytosolic DNA sensor STING (stimulator of IFN genes protein) (54). Of the four inhibitors used, only C16, targeting PKR, could substantially reduce the type I IFN response associated with *PSMC3* variants in these patients (Fig. 8B). These data thus suggest PKR as a sensor of

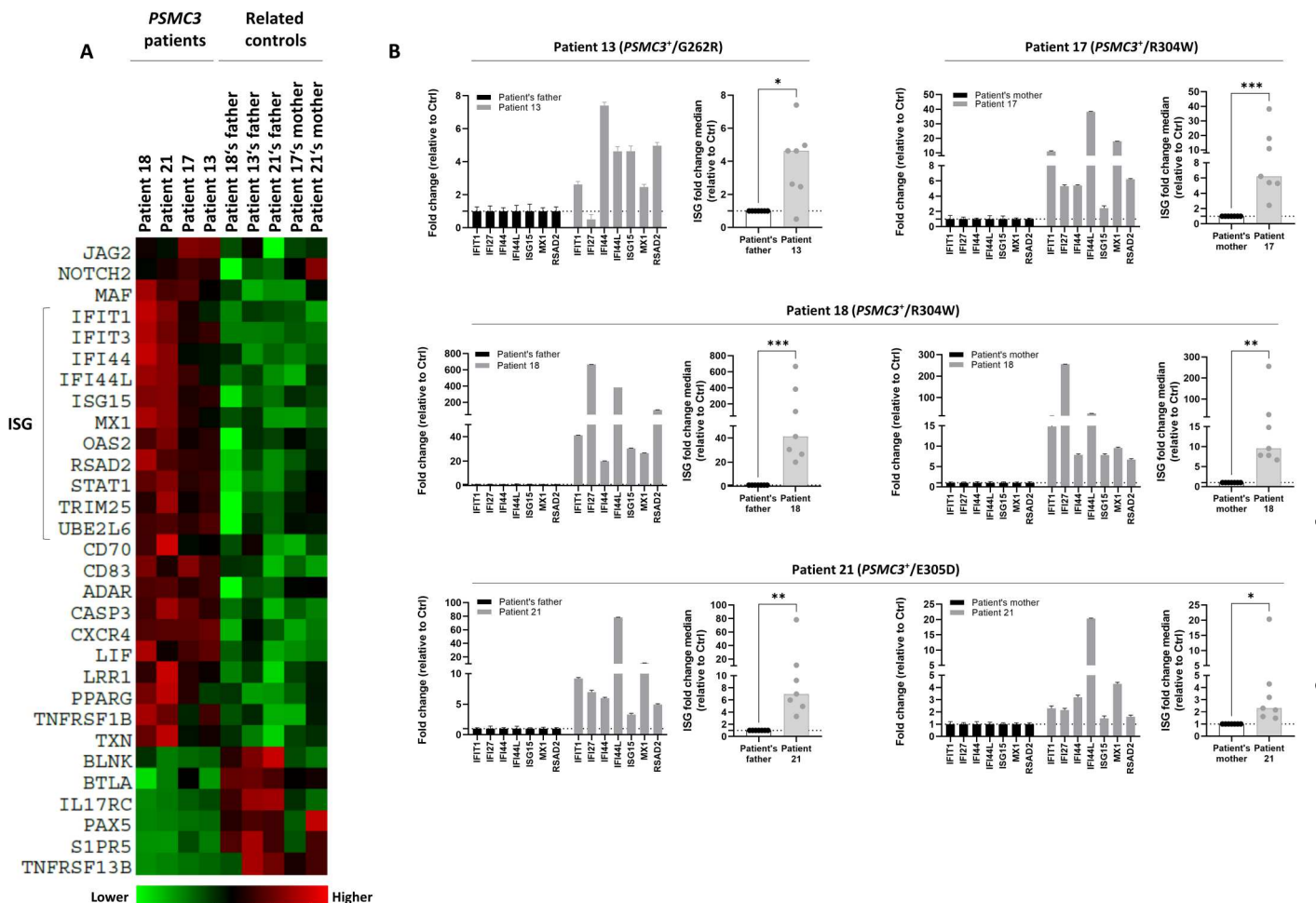


Fig. 7. T cells from patients with *PSMC3/Rpt5* **missense variants exhibit a type I IFN signature.** (**A**) Heatmap clustering of gene expression in T cells isolated from patients carrying a *PSMC3* variant and their relative controls (father, mother, or both). Each column represents one individual patient or related control, and each row represents one gene. Clustering of genes and samples was carried out by centered Pearson correlation. Color indicates normalized counts of each transcript, with green representing higher expression and red representing relatively lower expression. (**B**) Gene expression of seven typical IFN-stimulated genes (*IFIT1, IFI27, IFI44, IFI44L, ISG15, MX1*, and *RSAD2*) was assayed by RT-qPCR on T cells derived from patients #13, #17, #18, and #21 and their respective controls (the index case's father and/or mother). Expression levels were normalized to *GAPDH*, and relative quantifications are presented as fold change over controls. The median fold expression of the seven ISGs over relative controls is also shown. Statistical significance was assessed by ratio paired *t* test (**P* < 0.05, ***P* < 0.01, and ****P* < 0.001).

proteasome dysfunction triggering a type I IFN signature in individuals carrying *PSMC3* variants.

DISCUSSION

In this study, we identified 15 missense variants in the *PSMC3* gene in 23 unrelated individuals with NDD/ID (Fig. 1, Table 1, and table S1) and showed that the 19S AAA-ATPase proteasome subunit PSMC3/Rpt5 is a critical protein for the development of the central nervous system (CNS). This notion is in line with previous reports showing that conditional inactivation of other 19S proteasome subunits (Psmc2/Rpt2 and Psmc4/Rpt3) in mice results in severe neuronal phenotypes with features of neurodegeneration and locomotor dysfunction (55, 56). Recently, a homozygous deep intronic variant creating a cryptic exon in the *PSMC3* gene was linked to a familial recessive neurosensory syndrome (57). However, given their distinct modes of inheritance and

pathogenesis, this recessive disorder observed in a single family and the dominant variants, which we describe, are likely two different clinical entities with only partial overlap of clinical and molecular disease phenotypes (57). This dichotomy between dominant and recessive disorders may, nevertheless, be too reductive, because our data show that the dominant *PSMC3* variants do not necessarily exert the same effects on proteasome expression, assembly, or both (Figs. 3A and 4B and Table 1). These variations make it difficult to classify dominant *PSMC3* variants according to their impact on cellular function without any in vitro functional studies.

There are several limitations to this study. Given the limited number of biological samples investigated, a correlation between genotype and cellular phenotype could not be established. In this regard, it should also be noted that the gene silencing in the *Drosophila* model does not completely reflect disease biology patients, given that gene product is still available. We can furthermore not fully exclude a recruitment bias in our patient dataset.

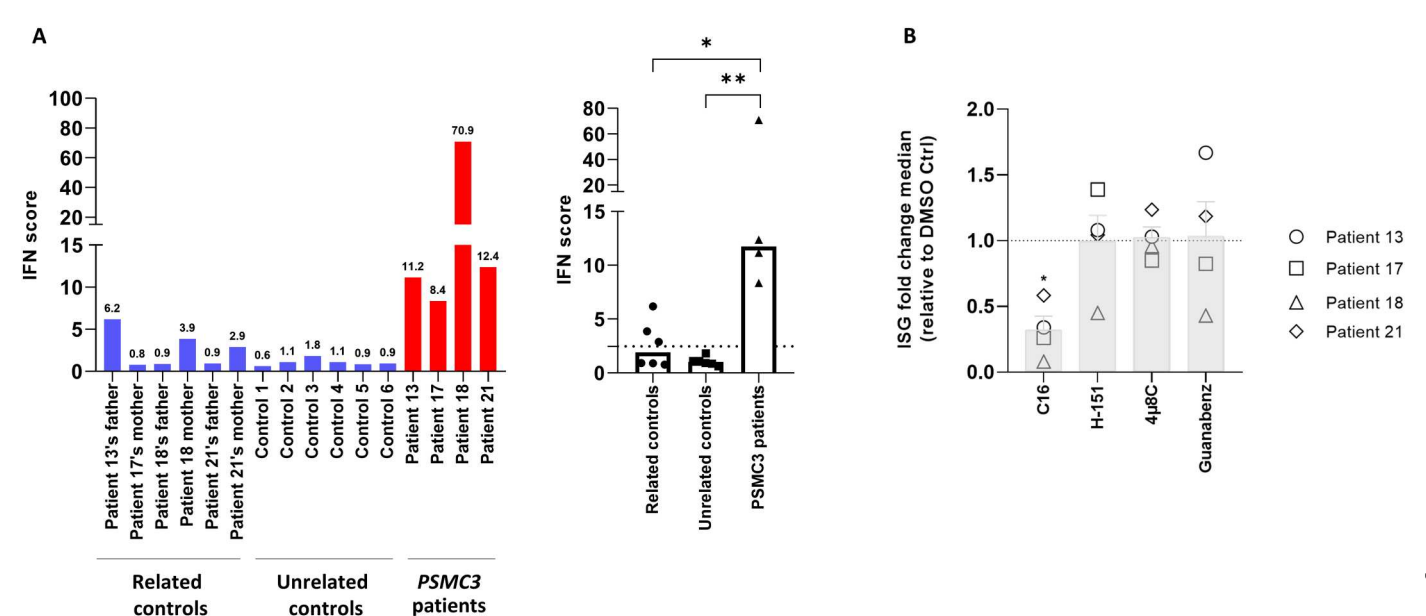


Fig. 8. T cells from patients with *PSMC3/Rpt5* missense variants exhibit high PKR dependent type I IFN scores. (A) Left: IFN scores for patients #13, #17, #18, and #21 and related controls as well as for six unrelated controls (1 to 6) were calculated as the median of the relative quantifications of the seven ISGs over a single calibrator control. The IFN scores of each sample (left) and the sample groups, namely, parents, unrelated healthy donors, and patients carrying *PSMC3* variants are shown, as indicated. Right: Box plot of concatenated data. Statistical significance was assessed by unpaired t test (*P < 0.05 and *P < 0.001). (B) T cells isolated from individuals carrying *PSMC3* variants were subjected to a 6-hour treatment with DMSO (vehicle), C16 (500 nM), H-151 (2 μ M), 4 μ 8C (100 μ M), or Guanabenz (50 μ M) inhibitors before RNA extraction and RT-qPCR for expression analysis of *IF127*, *IF144L*, *IFIT1*, *ISG15*, *RSAD2*, *IF144*, *OASL*, and *MX1*. Transcript expression was normalized to *GAPDH*, and data are presented as the fold change median values of the eight ISGs relative to DMSO (grid line) for each patient in each treatment. Columns indicate the fold change mean values \pm SEM of the patient group (N = 4) for each treatment. Statistical significance was assessed by ratio paired t test (*t < 0.05).

Cognitive flexibility is an important aspect of typical brain function, which allows adaptation to both physical and social environmental changes (58, 59). This may be assessed by evaluating reversal learning performance, a process that was initially identified in Drosophila models (60) and whose dysfunction has been associated with the pathogenesis of various neuropsychiatric disorders (61-65). Although Rpt5 gene silencing in flies had no discernible effect on learning performance, it led to compromised reversal learning (Fig. 2). Although proteasomes have been shown to regulate long-term potentiation (LTP) (66, 67), their involvement in reversal learning has not previously been shown. Our data identify PSMC3/Rpt5 as a key regulator of this process, whose molecular landscape was initially limited to a few molecules related to the cytoskeleton and GABAergic system (68–70). One cannot exclude that Rpt5 gene silencing in Drosophila may result in global depletion of 26S complexes, which, in turn, impairs reversal learning. However, some of the missense mutations identified in this study led to decreased PSMC3/Rpt5 expression (Fig. 3A), reduced incorporation into 26S complexes (Fig. 4B), or both, suggesting that a shortage of the PSMC3/Rpt5 subunit may reflect disease pathogenesis. The mechanisms by which proteasomes regulate reversal learning are unclear but may imply the degradation of specific neuronal proteins to control some synaptic connections and "reset" learning associations. It is tempting to speculate that one of these substrates could be Arc (activity-regulated cytoskeleton-associated protein), a key mediator of synaptic plasticity whose persistent expression has recently been shown to interfere with the reversal learning process (71). Additional evidence in favor of a critical role of PSMC3/Rpt5 in behavioral flexibility emerged from our experiments in primary

hippocampal neurons, showing that ectopic expression of PSMC3/Rpt5 affected dendrite growth (fig. S3). The observation that the R304W, E305D, and E383L PSMC3 variants did not differ from their WT counterpart in this process is intriguing but may have several explanations. First, WT PSMC3 overexpression may exert ceiling effects that overshadow any potential detrimental impact of the PSMC3 variants on neuronal morphology. Second, it may be that PSMC3 variants, with the exception of M159V, have no substantial effect on neuronal morphology. The reasons why the M159V PSMC3 variant behaves differently are unclear, but these findings might be explained by distinct half-life, intracellular localization, or posttranslational modifications. One could also argue that the adverse effects of PSMC3/Rpt5 on this process might be due to extra-proteasome functions as a consequence of an excess of "free" subunits after transfection. However, our investigations on patient T cells showed that PSMC3 missense variants were associated with an increased accumulation of ubiquitin-modified proteins (Fig. 6A), suggesting that these alterations give rise to proteasome loss-of-function variants associated with perturbed protein homeostasis. Future functional studies involving a larger number of biological samples are required to evaluate a possible correlation between PSMC3 variants and the extent of intracellular proteolysis dysfunction as a prerequisite for predicting disease severity.

Our proteomic analysis revealed that T cells from patients carrying *PSMC3* variants were enriched with ribosomal proteins such as RPL4, RPL6, RPL7A, and RPL7 (Fig. 5 and Table 2). These proteins may be specifically targeted for degradation, and their accumulation may occur as a consequence of impaired intracellular protein

clearance. Consistent with this notion, proteasome inhibition has been recently shown to result in the aggregation of ubiquitin-modified ribosomal proteins (72). Our data therefore support the recent view that ribosome dysregulation defines a key feature of NDD/ID phenotypes (73, 74) and the concept of translational arrest upon proteotoxic stress via the action of eIF2 α kinases (Fig. 6A).

One key finding is the observation that patients with PSMC3 variants generate a type I IFN gene signature (Figs. 7 and 8A). Although it is well established that proteasome loss-of-function variants cause interferonopathies in patients with PRAAS (27-33), it was only recently that pathogenic mutations in the 19S regulatory particle subunit PSMD12/Rpn5 were reported to engage constitutive type I IFN signaling in patients with this NDD disorder (35, 36) sharing similarities with the patients described in this manuscript. Although patients with PRAAS and individuals with NDD/ ID and PSMD12 or PSMC3 variants carry genomic alterations that affect the same multisubunit enzyme (26S proteasome), their clinical phenotypes do not entirely overlap. For instance, patients with NDD/ID and PSMC3 variants did not develop recurrent fever, lipodystrophy, and/or skin lesions, which are usually detected in patients with PRAAS (Table 1). One could argue that such differences may reflect distinct localizations of the affected subunits within the 26S proteasome complex, thereby suggesting that alterations of the 19S regulatory particle promote the generation of NDD/ID, whereas those of the 20S core particle or assembly chaperones favor the development a PRAAS phenotype. This assumption is, however, challenged by the fact that PSMB1/β6 variants of the 20S core particle lead to the acquisition of a neuronal phenotype very similar to that observed in patients with NDD/ID and PSMC3 variants (25). The lack of systemic autoinflammation in patients with NDD/ID and PSMC3 variants mounting a constitutive type I IFN response may seem surprising at first sight, but it is not totally unexpected, because this inconsistency is found in other NDDs, including Aicardi-Goutières (75, 76) and Down syndrome (77, 78). This is particularly well exemplified in patients with Down syndrome who, similar to patients with NDD/ID and PSMC3 dominant variants, exhibit a constitutive activation of type I IFN signaling (79, 80). To what extent type I IFN actively contributes to the pathogenesis of these disorders remains to be fully determined, although a growing body of evidence supports the notion that IFN has detrimental effects on CNS function (81-84) as well as stem cell function and differentiation (85, 86). Because proteasome dysfunction typically engages stress responses involving compensatory mechanisms such as autophagy (87), ISR, and UPR (24, 88), we reasoned that the type I IFN response detected in patients with PSMC3 variants might be triggered by sustained activation of either one of these pathways. As anticipated, high expression of autophagy and ER stress markers was detected in affected individuals, as evidenced by increased expression of the LC3-II and GRP94 proteins (Fig. 6, A and B). Both PINK1 and NIX mitochondrial proteins were found to be decreased in affected individuals (Fig. 6B), suggesting that PSMC3 variants increase autophagy-driven elimination of mitochondria (mitophagy). This observation supports the growing consensus that mitochondrial dysfunction is a key determinant of the pathogenesis of neurodevelopment (89) and the cause of interferonopathies (90). The activation status of PKR, a protein of the ISR that intersects with the UPR (91), was substantially increased in all investigated patients carrying the PSMC3 variant. Both ISR and UPR have the ability to counterbalance proteotoxic stress by inducing a global translational

arrest via eIF2α phosphorylation. This is accompanied by concomitant accumulation of nontranslated mRNAs, the formation of stress granules recruiting different RNA species, and RNA-processing enzymes, and IRE1-dependent mRNA decay (RIDD) (92). Although PKR typically responds to viral double-stranded RNA (93), it also may undergo activation under sterile conditions upon different stresses, including ER stress involving PKR-associated activator (PACT) and its modulator TAR RNA binding protein 2 (TRBP), a protein required for microRNA biogenesis (94-96). Both PACT and TRBP were observed to be increased in patient cells along with several RNA-processing factors. Our inhibition experiments suggested PKR as the inducer of type I IFN in these patients (Fig. 8B). The mechanisms by which PSMC3 variants activate PKR in affected individuals remain unclear, but our data open the possibility that PKR may sense a broader spectrum of danger signals than initially assumed, including perturbations of protein homeostasis. This concept is in line with the observation that activated PKR was found in the CNS of patients with neurodegenerative diseases (97-100) and that neurodegeneration is associated with neuroinflammation (101, 102). Together, our work demonstrates that heterozygous PSMC3 dominant variants result in a neurodevelopmental syndrome associated with a specific type I IFN gene signature and suggests treatment options targeting type I IFN signaling or PKR.

MATERIALS AND METHODS

Study design

The aim of the study was to determine the involvement of the human PSMC3 gene in a neurodevelopmental disorder hitherto unreported. Affected individuals were recruited, and data were collected on an ongoing basis. Affected individuals were identified via the data sharing platform GeneMatcher (103) and direct requests in variants databases whose access was authorized to the University of Washington School of Medicine. Clinical and molecular data were provided by the referring geneticists following the patients. Facial recognition by GestaltMatcher (41) was used to measure the similarities of the facial phenotypes between affected individuals (fig. S2). Prediction of variant pathogenicity was done using the bioinformatics programs indicated in Table 1, and their frequency was determined in public variant databases [gnomAD; (104), Exome Variant Server, NHLBI GO Exome Sequencing Project (ESP), Seattle, WA (http://evs.gs.washington.edu/EVS/) (accessed March 2023); Bravo powered by TOPMed Freeze 8 on GRCh38 (105)]. The effects of the *PSMC3* variants on proteasome function, protein homeostasis, proteotoxic stress sensors (UPR and ISR), autophagy/mitophagy, and inflammation status (type I IFN) were studied in vitro by Western blotting, NanoString analysis, and quantitative PCR (qPCR) using T cells expanded from wholeblood samples of patients (N = 4) and their parents (N = 6) who agreed to provide blood specimens. The first available T cell samples (patients N = 2, related controls N = 2) were used for proteomics analyses to explore deregulated biological pathways. The impact of the variants on neuronal function was assessed in two models: (i) upstream activation sequence-Rpt5 RNAi D. melanogaster lines targeting psmc3 for evaluating the effect of Rpt5 knockdown on behavior (Fig. 2) and (ii) primary hippocampal neuronal cultures overexpressing cDNA constructs containing the first identified variants (N = 4) for evaluating their effects on neuronal

PG.Protein Groups	Protein name	Gene name	Mut/Co signal_log2_ratio	Mut/Co raw_p_value	Mut/Co adjusted_p_value
P02749	Beta-2-glycoprotein 1	APOH	3.90875773	3.9233×10^{-05}	0.01752392
P01861	lmmunoglobulin heavy constant gamma 4	IGHG4	3.41081457	3.9313×10^{-07}	0.0003951
Q02878	60S ribosomal protein L6	RPL6	3.09519982	8.1085×10^{-05}	0.02173071
P62424	60S ribosomal protein L7a	RPL7A	2.97520531	2.4946×10^{-06}	0.00143263
P18124	60S ribosomal protein L7	RPL7	2.90834996	5.5264×10^{-05}	0.01815176
P83731	60S ribosomal protein L24	RPL24	2.78639617	5.8732×10^{-05}	0.01815176
P16403	Histone H1.2	H1-2	2.72232694	4.4042×10^{-05}	0.0177049
P02768	Serum albumin	ALB	2.64236248	3.3722×10^{-18}	1.3556×10^{-14}
P36578	60S ribosomal protein L4	RPL4	2.50022766	3.276×10^{-07}	0.0003951
P01876	lmmunoglobulin heavy constant alpha 1	IGHA1	2.32067402	3.007×10^{-05}	0.01511011
P20591	IFN-induced GTP-binding protein Mx1	MX1	2.20162951	6.3215 × 10 ⁻⁰⁵	0.01815176
Q6P2Q9	Pre-mRNA-processing-splicing factor 8	PRPF8	1.33941179	1.5549 × 10 ⁻⁰⁶	0.00125012
Q01469	Fatty acid-binding protein 5	FABP5	-2.29088412	5.7962 × 10 ⁻⁰⁵	0.01815176

morphology (fig. S3). Details about data replication are provided in the figure legends. Experimenters were not blinded.

Human participants

All affected participants were initially referred for unexplained DD and/or ID together with various congenital malformations. They underwent extensive clinical examination by at least one clinical geneticist participating in the study. Routine genetic testing was performed whenever clinically relevant, including copy number variation analysis by high-resolution array-based comparative genomic hybridization. Because these tests failed to establish the diagnosis of a specific disease, trio-based WES was performed in a diagnostic or research setting whenever parental samples were available. Because disorders associated with PSMC3 are very rare, the reported patient cohort is representative of cases identified worldwide over the past 6 years and is not, for example, a selection of a subgroup of a larger patient population. This study was approved by the CHU de Nantes ethics committee (Research Programme "Génétique Médicale DC-2011-1399). Probands 2, 5 to 10, 12 to 14, 16 to 18, and 20 to 23 were enrolled by one of the participating centers [Washington University in St. Louis, University Medical Centre of Utrecht, University Hospital Center of Nantes, Arnold Palmer Hospital, Seattle Children's Hospital, St. Luke's Hospital, Health San Antonio, Vanderbilt University Medical Center, Sydney Medical School, Children's Hospital of Philadelphia, Technical University of Munich, Pitié-Salpêtrière University Hospital, Children's Hospital of Orange County, Ambry Genetics, Geisinger Medical Center, Guy's and St Thomas' NHS Foundation Trust, McGill University Health Centre, Nottingham University Hospitals NHS Trust, Hôpital Universitaire Necker-Enfants Malades, University Children's Hospital, Salzburger Landeskliniken (SALK), and Paracelsus Medical University after approval of genetic studies by local ethics committees. Written informed consent was obtained from all study participants, including probands and healthy parents. All affected individuals were initially referred for unexplained DD and/or ID together with various congenital malformations. They underwent extensive clinical examination by at least one expert clinical geneticist. Individuals 1, 4, 11, 15, and 19 participated in "Simons Foundation Powering Autism Research" (SPARK) or "Deciphering Developmental Disorders" (DDD) initiative; clinical information about individuals 1, 3, and 14 was retrieved by members of the University of Washington School of Medicine in agreement with SPARK and DDD.

Cell culture

Peripheral blood mononuclear cells (PBMCs) used in this paper were isolated from blood draws from patients and related healthy controls (father and/or mother of the proband). Briefly, PBMCs were isolated by PBMC spin medium gradient centrifugations (pluriSelect), washed three times with phosphate-buffered saline (PBS), frozen in fetal bovine serum with 10% dimethyl sulfoxide (DMSO), and stored in liquid nitrogen for further use. In some experiments, collected PBMCs were expanded in U-bottom 96-well plates together with feeder cells using RPMI 1640 supplemented with 10% human AB serum (both purchased from PAN-Biotech GmbH) in the presence of IL-2 (150 U/ml; Miltenyi Biotec) and L-PHA (1 μ g/ μ l; Sigma-Aldrich) following the procedure of Fonteneau *et al.* (106). After 3 to 4 weeks of culture, resting T cells were washed and frozen as dry pellets for further use.

SDS-PAGE and western-blot analysis

Cell pellets from resting T cells isolated from patients and related controls were lysed in equal amounts of standard radioimmunoprecipitation assay buffer [50 mM tris (pH 7.5), 150 mM NaCl, 2 mM EDTA, 1 mM N-ethylmaleimide, 10 μ M MG-132, 1% NP-40, and 0.1% SDS] and separated by 10 or 12.5% SDS-PAGE before transfer to polyvinylidene difluoride membranes (200 V for 1 hour). After blocking (20-min exposure to 1X Roti-Block at room temperature),

membranes were probed with relevant primary antibodies overnight at 4°C under shaking. The anti-α6 (clone MCP20), anti-α7 (clone MCP72), anti-β1 (clone MCP421), anti-PSMC2 (BML-PW8315), and anti-PSMC3 (BML-PW8310) primary antibodies were purchased from Enzo Life Sciences. Primary antibodies specific for TCF11/Nrf1 (clone D5B10), ubiquitin (clone D9D5), glyceraldehyde phosphate dehydrogenase (GAPDH) (clone 14C10), PINK1 (clone D8G3), BNIP3L/NIX (clone D8G3), LC3b (#2775), eIF2 α (#9722), phospho-eIF2 α (Ser⁵¹, #119A11) were obtained from Cell Signaling Technology. The anti-PSMD12 antibody (clone H3) was a purchase from Santa Cruz Biotechnology Inc. The anti–PA28-α (K232/1) is laboratory stock and was used in previous studies (31). Antibodies directed against β5 (ab3330), αtubulin (clone DM1A), and phospho-PKR (Thr446, clone E120) were purchased from Abcam. After incubation with primary antibodies, membranes were washed three times with PBS/0.2% Tween and subsequently incubated with anti-mouse or anti-rabbit horseradish peroxidase-conjugated secondary antibodies (1:5000) for 1 hour at room temperature. Proteins were then visualized using an enhanced chemiluminescence detection kit (Bio-Rad).

RNA isolation, RT, and PCR analysis

Total RNA was isolated from resting T cells using the kit from Analytic Jena AG following the manufacturer's instructions. For subsequent real-time PCR, 100 to 500 ng of the isolated total RNA were reverse-transcribed using the M-MLV reverse transcriptase (Promega). qPCR was performed using the Premix Ex Taq (probe qPCR purchased from TaKaRa) and in duplicates to determine the mRNA expression of each ISG using FAM-tagged TaqMan Gene Expression Assays obtained from Thermo Fisher Scientific according to the manufacturer's instructions. TaqMan probes used in this study for ISG quantification included *IFI27*, *IFI44L*, *IFIT1*, *ISG15*, *RSAD2*, *IFI44*, *MX1*, *OASL1*, *CXCL9*, and *CXCL10*. The cycle threshold (Ct) values for target genes were converted to values of relative expression using the relative quantification method ($2^{-\Delta \Delta Ct}$). Target gene expression was calculated relative to Ct values for the GAPDH control housekeeping gene.

Statistical analyses

Figures were created with PyMOL version 2.0 (pymol.org) using the human 26S proteasome structure. Data are typically median or means \pm SEM and were analyzed by unpaired and pair ratio t test between two groups. Neuronal morphology data were analyzed using a one-way analysis of variance (ANOVA), followed by a Tukey's post hoc test for multiple comparisons. All charts and statistical analyses were generated using GraphPad Prism version 8. A P value < 0.05 was considered significant.

Supplementary Materials

This PDF file includes: Materials and Methods Fig. S1 to S14 Table S1 References (107–116)

Other Supplementary Material for this manuscript includes the following:
Data files S1 and S2
MDAR Reproducibility Checklist

View/request a protocol for this paper from Bio-protocol.

REFERENCES AND NOTES

- K. Tanaka, T. Mizushima, Y. Saeki, The proteasome: Molecular machinery and pathophysiological roles. *Biol. Chem.* 393, 217–234 (2012).
- 2. G. A. Collins, A. L. Goldberg, The logic of the 26S proteasome. Cell 169, 792–806 (2017).
- 3. M. W. Hetzer, B. H. Toyama, Protein homeostasis: Live long, won't prosper. *Nat. Rev. Mol. Cell Biol.* **14**, 55–61 (2013).
- P. Goloubinoff, Mechanisms of protein homeostasis in health, aging and disease. Swiss Med. Wkly. 146, w14306 (2016).
- U. Seifert, L. P. Bialy, F. Ebstein, D. Bech-Otschir, A. Voigt, F. Schröter, T. Prozorovski, N. Lange, J. Steffen, M. Rieger, U. Kuckelkorn, O. Aktas, P.-M. Kloetzel, E. Krüger, Immunoproteasomes preserve protein homeostasis upon interferon-induced oxidative stress. Cell 142, 613–624 (2010).
- E. Krüger, P. M. Kloetzel, Immunoproteasomes at the interface of innate and adaptive immune responses: Two faces of one enzyme. Curr. Opin. Immunol. 24, 77–83 (2012).
- C. M. Pickart, Mechanisms underlying ubiquitination. Annu. Rev. Biochem. 70, 503–533 (2001).
- G. N. DeMartino, T. G. Gillette, Proteasomes: Machines for all reasons. Cell 129, 659–662 (2007).
- C. M. Pickart, D. Fushman, Polyubiquitin chains: Polymeric protein signals. Curr. Opin. Chem. Biol. 8, 610–616 (2004).
- 10. C. M. Pickart, Back to the Future with Ubiquitin. Cell 116, 181-190 (2004).
- K. Tanaka, The proteasome: Overview of structure and functions. Proc. Jpn. Acad. Ser. B Phys. Biol. Sci. 85, 12–36 (2009).
- B. Dahlmann, Mammalian proteasome subtypes: Their diversity in structure and function. *Arch. Biochem. Biophys.* 591, 132–140 (2016).
- R. J. Tomko, M. Funakoshi, K. Schneider, J. Wang, M. Hochstrasser, Heterohexameric ring arrangement of the eukaryotic proteasomal ATPases: Implications for proteasome structure and assembly. Mol. Cell 38, 393–403 (2010).
- D. M. Smith, S. C. Chang, S. Park, D. Finley, Y. Cheng, A. L. Goldberg, Docking of the proteasomal ATPases' carboxyl termini in the 20S proteasome's α ring opens the gate for substrate entry. *Mol. Cell* 27, 731–744 (2007).
- E. R. Greene, K. C. Dong, A. Martin, Understanding the 26S proteasome molecular machine from a structural and conformational dynamics perspective. *Curr. Opin. Struct. Biol.* 61, 33–41 (2020).
- E. R. Greene, E. A. Goodall, A. H. de la Peña, M. E. Matyskiela, G. C. Lander, A. Martin, Specific lid-base contacts in the 26S proteasome control the conformational switching required for substrate degradation. *eLife* 8, e49806 (2019).
- R. Verma, L. Aravind, R. Oania, W. H. McDonald, J. R. Yates, E. V. Koonin, R. J. Deshaies, Role of Rpn11 metalloprotease in deubiquitination and degradation by the 26S proteasome. *Science* 298, 611–615 (2002).
- A. F. Kisselev, W. A. van der Linden, H. S. Overkleeft, Proteasome inhibitors: An expanding army attacking a unique target. Chem. Biol. 19, 99–115 (2012).
- D. Finley, X. Chen, K. J. Walters, Gates, channels, and switches: Elements of the proteasome machine. *Trends Biochem. Sci.* 41, 77–93 (2016).
- F. Ebstein, P.-M. Kloetzel, E. Krüger, U. Seifert, Emerging roles of immunoproteasomes beyond MHC class I antigen processing. Cell. Mol. Life Sci. 69, 2543–2558 (2012).
- B. Strehl, U. Seifert, E. Krüger, S. Heink, U. Kuckelkorn, P.-M. Kloetzel, Interferon-γ, the functional plasticity of the ubiquitin–proteasome system, and MHC class I antigen processing. *Immunol. Rev.* 207, 19–30 (2005).
- E. C. Shin, U. Seifert, S. Urban, K. T. Truong, S. M. Feinstone, C. M. Rice, P. M. Kloetzel,
 B. Rehermann, Proteasome activator and antigen-processing aminopeptidases are regulated by virus-induced type I interferon in the hepatitis C virus-infected liver. *J. Interferon Cytokine Res.* 27, 985–990 (2007).
- 23. A. Brehm, E. Krüger, Dysfunction in protein clearance by the proteasome: Impact on autoinflammatory diseases. *Semin. Immunopathol.* **37**, 323–333 (2015).
- F. Ebstein, M. C. Poli Harlowe, M. Studencka-Turski, E. Krüger, Contribution of the unfolded protein response (UPR) to the pathogenesis of proteasome-associated autoinflammatory syndromes (PRAAS). Front. Immunol. 10, 2756 (2019).
- M. Ansar, F. Ebstein, H. Özkoç, S. A. Paracha, J. Iwaszkiewicz, M. Gesemann, V. Zoete, E. Ranza, F. A. Santoni, M. T. Sarwar, J. Ahmed, E. Krüger, R. Bachmann-Gagescu, S. E. Antonarakis, Biallelic variants in PSMB1 encoding the proteasome subunit β6 cause impairment of proteasome function, microcephaly, intellectual disability, developmental delay and short stature. *Hum. Mol. Genet.* 29, 1132–1143 (2021).
- A. K. Agarwal, C. Xing, G. N. Demartino, D. Mizrachi, M. D. Hernandez, A. B. Sousa, L. Martínez De Villarreal, H. G. dos Santos, A. Garg, PSMB8 encoding the β5i proteasome subunit is mutated in joint contractures, muscle atrophy, microcytic anemia, and panniculitis-induced lipodystrophy syndrome. Am. J. Hum. Genet. 87, 866–872 (2010).

SCIENCE TRANSLATIONAL MEDICINE | RESEARCH ARTICLE

- K. Arima, A. Kinoshita, H. Mishima, N. Kanazawa, T. Kaneko, T. Mizushima, K. Ichinose, H. Nakamura, A. Tsujino, A. Kawakami, M. Matsunaka, S. Kasagi, S. Kawano, S. Kumagai, K. Ohmura, T. Mimori, M. Hirano, S. Ueno, K. Tanaka, M. Tanaka, I. Toyoshima, H. Sugino, A. Yamakawa, K. Tanaka, N. Niikawa, F. Furukawa, S. Murata, K. Eguchi, H. Ida, K. I. Yoshiura, Proteasome assembly defect due to a proteasome subunit beta type 8 (PSMB8) mutation causes the autoinflammatory disorder, Nakajo-Nishimura syndrome. *Proc. Natl. Acad. Sci.* U.S.A. 108, 14914–14919 (2011).
- A. Kitamura, Y. Maekawa, H. Uehara, K. Izumi, I. Kawachi, M. Nishizawa, Y. Toyoshima, H. Takahashi, D. M. Standley, K. Tanaka, J. Hamazaki, S. Murata, K. Obara, I. Toyoshima, K. Yasutomo, A mutation in the immunoproteasome subunit PSMB8 causes autoinflammation and lipodystrophy in humans. J. Clin. Invest. 121, 4150–4160 (2011).
- Y. Liu, Y. Ramot, A. Torrelo, A. S. Paller, N. Si, S. Babay, P. W. Kim, A. Sheikh, C.-C. R. Lee, Y. Chen, A. Vera, X. Zhang, R. Goldbach-Mansky, A. Zlotogorski, Mutations in proteasome subunit β type 8 cause chronic atypical neutrophilic dermatosis with lipodystrophy and elevated temperature with evidence of genetic and phenotypic heterogeneity. Arthritis Rheum. 64, 895–907 (2012).
- A. Brehm, Y. Liu, A. Sheikh, B. Marrero, E. Omoyinmi, Q. Zhou, G. Montealegre, A. Biancotto, A. Reinhardt, A. A. de Jesus, M. Pelletier, W. L. Tsai, E. F. Remmers, L. Kardava, S. Hill, H. Kim, H. J. Lachmann, A. Megarbane, J. J. Chae, J. Brady, R. D. Castillo, D. Brown, A. V. Casano, L. Gao, D. Chapelle, Y. Huang, D. Stone, Y. Chen, F. Sotzny, C. C. R. Lee, D. L. Kastner, A. Torrelo, A. Zlotogorski, S. Moir, M. Gadina, P. McCoy, R. Wesley, K. Rother, P. W. Hildebrand, P. Brogan, E. Krüger, I. Aksentijevich, R. Goldbach-Mansky, Additive loss-of-function proteasome subunit mutations in CANDLE/PRAAS patients promote type I IFN production. J. Clin. Invest. 125, 4196–4211 (2015).
- 31. M. C. Poli, F. Ebstein, S. K. Nicholas, M. M. de Guzman, L. R. Forbes, I. K. Chinn, E. M. Mace, T. P. Vogel, A. F. Carisey, F. Benavides, Z. H. Coban-Akdemir, R. A. Gibbs, S. N. Jhangiani, D. M. Muzny, C. M. B. Carvalho, D. A. Schady, M. Jain, J. A. Rosenfeld, L. Emrick, R. A. Lewis, B. Lee, B. A. Zieba, S. Küry, E. Krüger, J. R. Lupski, B. L. Bostwick, J. S. Orange, Heterozygous truncating variants in *POMP* escape nonsense-mediated decay and cause a unique immune dysregulatory syndrome. *Am. J. Hum. Genet.* 102, 1126–1142 (2018).
- A. A. de Jesus, A. Brehm, R. VanTries, P. Pillet, A. S. Parentelli, G. A. Montealegre Sanchez,
 Z. Deng, I. K. Paut, R. Goldbach-Mansky, E. Krüger, Novel Proteasome Assembly Chaperone mutations in PSMG2/PAC2 cause the autoinflammatory interferonopathy CANDLE/PRAAS4. J. Allergy Clin. Immunol. 143, 1939–1943.e8 (2019).
- G. Sarrabay, D. Méchin, A. Salhi, G. Boursier, C. Rittore, Y. Crow, G. Rice, T. A. Tran, R. Cezar, D. Duffy, V. Bondet, L. Boudhane, C. Broca, B. P. Kant, M. VanGijn, S. Grandemange, E. Richard, F. Apparailly, I. Touitou, PSMB10, the last immunoproteasome gene missing for PRAAS. J. Alleray Clin. Immunol. 145. 1015–1017.e6 (2020).
- S. Küry, T. Besnard, F. Ebstein, T. N. Khan, T. Gambin, J. Douglas, C. A. Bacino, S. J. Sanders, A. Lehmann, X. Latypova, K. Khan, M. Pacault, S. Sacharow, K. Glaser, E. Bieth, L. Perrin-Sabourin, M.-L. Jacquemont, M. T. Cho, E. Roeder, A.-S. Denommé-Pichon, K. G. Monaghan, B. Yuan, F. Xia, S. Simon, D. Bonneau, P. Parent, B. Gilbert-Dussardier, S. Odent, A. Toutain, L. Pasquier, D. Barbouth, C. A. Shaw, A. Patel, J. L. Smith, W. Bi, S. Schmitt, W. Deb, M. Nizon, S. Mercier, M. Vincent, C. Rooryck, V. Malan, I. Briceño, A. Gómez, K. M. Nugent, J. B. Gibson, B. Cogné, J. R. Lupski, H. A. F. Stessman, E. E. Eichler, K. Retterer, Y. Yang, R. Redon, N. Katsanis, J. A. Rosenfeld, P.-M. Kloetzel, C. Golzio, S. Bézieau, P. Stankiewicz, B. Isidor, De novo disruption of the proteasome regulatory subunit PSMD12 causes a syndromic neurodevelopmental disorder. Am. J. Hum. Genet. 100, 352–363 (2017).
- B. Isidor, F. Ebstein, A. Hurst, M. Vincent, I. Bader, N. L. Rudy, B. Cogne, J. Mayr, A. Brehm, C. Bupp, K. Warren, C. A. Bacino, A. Gerard, J. D. Ranells, K. A. Metcalfe, Y. van Bever, Y. H. Jiang, B. A. Mendelssohn, H. Cope, J. A. Rosenfeld, P. R. Blackburn, M. L. Goodenberger, H. M. Kearney, J. Kennedy, I. Scurr, K. Szczaluba, R. Ploski, A. de Saint Martin, Y. Alembik, A. Piton, A. L. Bruel, C. Thauvin-Robinet, A. Strong, K. E. M. Diderich, D. Bourgeois, K. Dahan, V. Vignard, D. Bonneau, E. Colin, M. Barth, C. Camby, G. Baujat, I. Briceño, A. Gómez, W. Deb, S. Conrad, T. Besnard, S. Bézieau, E. Krüger, S. Küry, P. Stankiewicz, Stankiewicz-Isidor syndrome: Expanding the clinical and molecular phenotype. Genet. Med. 24, 179–191 (2022).
- K. Yan, J. Zhang, P. Y. Lee, P. Tao, J. Wang, S. Wang, Q. Zhou, M. Dong, Haploinsufficiency of PSMD12 causes proteasome dysfunction and subclinical autoinflammation. *Arthritis Rheumatol.* 74, 1083–1090 (2022).
- 37. D. M. d'Angelo, P. di Filippo, L. Breda, F. Chiarelli, Type I interferonopathies in children: An overview. *Front. Pediatr.* **9**, 631329 (2021).
- S. Savic, J. Coe, P. Laws, Autoinflammation: Interferonopathies and other autoinflammatory diseases. J. Invest. Dermatol. 142, 781–792 (2022).
- Y. J. Crow, D. B. Stetson, The type I interferonopathies: 10 years on. Nat. Rev. Immunol. 22, 471–483 (2022).
- D. Baux, C. van Goethem, O. Ardouin, T. Guignard, A. Bergougnoux, M. Koenig, A. F. Roux, MobiDetails: Online DNA variants interpretation. *Eur. J. Hum. Genet.* 29, 356–360 (2021).

- T. C. Hsieh, A. Bar-Haim, S. Moosa, N. Ehmke, K. W. Gripp, J. T. Pantel, M. Danyel, M. A. Mensah, D. Horn, S. Rosnev, N. Fleischer, G. Bonini, A. Hustinx, A. Schmid, A. Knaus, B. Javanmardi, H. Klinkhammer, H. Lesmann, S. Sivalingam, T. Kamphans, W. Meiswinkel, F. Ebstein, E. Krüger, S. Küry, S. Bézieau, A. Schmidt, S. Peters, H. Engels, E. Mangold, M. Kreiß, K. Cremer, C. Perne, R. C. Betz, T. Bender, K. Grundmann-Hauser, T. B. Haack, M. Wagner, T. Brunet, H. B. Bentzen, L. Averdunk, K. C. Coetzer, G. J. Lyon, M. Spielmann, C. P. Schaaf, S. Mundlos, M. M. Nöthen, P. M. Krawitz, GestaltMatcher facilitates rare disease matching using facial phenotype descriptors. *Nat. Genet.* 54, 349–357 (2022).
- T. Tully, W. G. Quinn, Classical conditioning and retention in normal and mutant Drosophila melanogaster. J. Comp. Physiol. A 157, 263–277 (1985).
- 43. S. Küry, G. M. van Woerden, T. Besnard, M. Proietti Onori, X. Latypova, M. C. Towne, M. T. Cho, T. E. Prescott, M. A. Ploeg, S. Sanders, H. A. F. Stessman, A. Pujol, B. Distel, L. A. Robak, J. A. Bernstein, A. S. Denommé-Pichon, G. Lesca, E. A. Sellars, J. Berg, W. Carré, Ø. L. Busk, B. W. M. van Bon, J. L. Waugh, M. Deardorff, G. E. Hoganson, K. B. Bosanko, D. S. Johnson, T. Dabir, Ø. L. Holla, A. Sarkar, K. Tveten, J. de Bellescize, G. J. Braathen, P. A. Terhal, D. K. Grange, A. van Haeringen, C. Lam, G. Mirzaa, J. Burton, E. J. Bhoj, J. Douglas, A. B. Santani, A. I. Nesbitt, K. L. Helbig, M. V. Andrews, A. Begtrup, S. Tang, K. L. I. van Gassen, J. Juusola, K. Foss, G. M. Enns, U. Moog, K. Hinderhofer, N. Paramasivam, S. Lincoln, B. H. Kusako, P. Lindenbaum, E. Charpentier, C. B. Nowak, E. Cherot, T. Simonet, C. A. L. Ruivenkamp, S. Hahn, C. A. Brownstein, F. Xia, S. Schmitt, W. Deb, D. Bonneau, M. Nizon, D. Quinquis, J. Chelly, G. Rudolf, D. Sanlaville, P. Parent, B. Gilbert-Dussardier, A. Toutain, V. R. Sutton, J. Thies, L. E. L. M. Peart-Vissers, P. Boisseau, M. Vincent, A. M. Grabrucker, C. Dubourg, W. H. Tan, N. E. Verbeek, M. Granzow, G. W. E. Santen, J. Shendure, B. Isidor, L. Pasquier, R. Redon, Y. Yang, M. W. State, T. Kleefstra, B. Cogné, S. Petrovski, K. Retterer, E. E. Eichler, J. A. Rosenfeld, P. B. Agrawal, S. Bézieau, S. Odent, Y. Elgersma, S. Mercier, De novo mutations in protein kinase genes CAMK2A and CAMK2B cause intellectual disability. Am. J. Hum. Genet. 101, 768-788 (2017).
- L. Schembri, R. Dalibart, F. Tomasello, P. Legembre, F. Ichas, F. de Giorgi, The HA tag is cleaved and loses immunoreactivity during apoptosis. *Nat. Methods* 4, 107–108 (2007).
- Y. Dong, S. Zhang, Z. Wu, X. Li, W. L. Wang, Y. Zhu, S. Stoilova-McPhie, Y. Lu, D. Finley, Y. Mao, Cryo-EM structures and dynamics of substrate-engaged human 26S proteasome. Nature 565. 49–55 (2019).
- M. D. Shmueli, D. Sheban, A. Eisenberg-Lerner, Y. Merbl, Histone degradation by the proteasome regulates chromatin and cellular plasticity. FEBS J. 289, 3304–3316 (2022).
- D. J. McConkey, The integrated stress response and proteotoxicity in cancer therapy. Biochem. Biophys. Res. Commun. 482, 450–453 (2017).
- 48. M. Marzec, D. Eletto, Y. Argon, GRP94: An HSP90-like protein specialized for protein folding and quality control in the endoplasmic reticulum. *Biochim. Biophys. Acta Mol. Cell Res.* **1823**, 774–787 (2012).
- S. K. Radhakrishnan, C. S. Lee, P. Young, A. Beskow, J. Y. Chan, R. J. Deshaies, Transcription factor Nrf1 mediates the proteasome recovery pathway after proteasome inhibition in mammalian cells. *Mol. Cell* 38, 17–28 (2010).
- J. Steffen, M. Seeger, A. Koch, E. Krüger, Proteasomal degradation is transcriptionally controlled by TCF11 via an ERAD-dependent feedback loop. Mol. Cell 40, 147–158 (2010).
- B. Kostyszyn, R. F. Cowburn, Å. Seiger, A. Kjældgaard, E. Sundström, Distribution of presenilin 1 and 2 and their relation to Notch receptors and ligands in human embryonic/ foetal central nervous system. *Brain Res. Dev. Brain Res.* 151, 75–86 (2004).
- G. I. Rice, I. Melki, M. L. Frémond, T. A. Briggs, M. P. Rodero, N. Kitabayashi, A. Oojageer,
 B. Bader-Meunier, A. Belot, C. Bodemer, P. Quartier, Y. J. Crow, Assessment of type I interferon signaling in pediatric inflammatory disease. J. Clin. Immunol. 37, 123–132 (2017).
- F. Ebstein, N. Lange, S. Urban, U. Seifert, E. Krüger, P. M. Kloetzel, Maturation of human dendritic cells is accompanied by functional remodelling of the ubiquitin-proteasome system. *Int. J. Biochem. Cell Biol.* 41, 1205–1215 (2009).
- A. Tesser, G. M. Piperno, A. Pin, E. Piscianz, V. Boz, F. Benvenuti, A. Tommasini, Priming of the cGAS-STING-TBK1 pathway enhances LPS-induced release of type I interferons. *Cell* 10, 785 (2021).
- L. Bedford, D. Hay, A. Devoy, S. Paine, D. G. Powe, R. Seth, T. Gray, I. Topham, K. Fone, N. Rezvani, M. Mee, T. Soane, R. Layfield, P. W. Sheppard, T. Ebendal, D. Usoskin, J. Lowe, R. J. Mayer, Depletion of 26S proteasomes in mouse brain neurons causes neurodegeneration and Lewy-like inclusions resembling human pale bodies. *J. Neurosci.* 28, 8189–8198 (2008).
- Y. Tashiro, M. Urushitani, H. Inoue, M. Koike, Y. Uchiyama, M. Komatsu, K. Tanaka, M. Yamazaki, M. Abe, H. Misawa, K. Sakimura, H. Ito, R. Takahashia, Motor neuron-specific disruption of proteasomes, but not autophagy, replicates amyotrophic lateral sclerosis. J. Biol. Chem. 287, 42984–42994 (2012).
- A. Kröll-Hermi, F. Ebstein, C. Stoetzel, V. Geoffroy, E. Schaefer, S. Scheidecker, S. Bär, M. Takamiya, K. Kawakami, B. A. Zieba, F. Studer, V. Pelletier, C. Eyermann, C. Speeg-Schatz, V. Laugel, D. Lipsker, F. Sandron, S. McGinn, A. Boland, J. Deleuze, L. Kuhn, J. Chicher, P. Hammann, S. Friant, C. Etard, E. Krüger, J. Muller, U. Strähle, H. Dollfus, Proteasome

SCIENCE TRANSLATIONAL MEDICINE | RESEARCH ARTICLE

- subunit PSMC3 variants cause neurosensory syndrome combining deafness and cataract due to proteotoxic stress. *EMBO Mol. Med.* **12.** e11861 (2020).
- 58. P. Reed, H. Watts, R. Truzoli, Flexibility in young people with autism spectrum disorders on a card sort task. *Autism* 17, 162–171 (2013).
- R. C. Leung, K. K. Zakzanis, Brief report: Cognitive flexibility in autism spectrum disorders: A quantitative review. J. Autism Dev. Disord. 44, 2628–2645 (2014).
- T. Tully, S. Boyton, C. Brandes, J. M. Dura, R. Mihalek, T. Preat, A. Villella, Genetic dissection of memory formation in Drosophila melanogaster. *Cold Spring Harb. Symp. Quant. Biol.* 55. 203–211 (1990).
- R. Swainson, R. D. Rogers, B. J. Sahakian, B. A. Summers, C. E. Polkey, T. W. Robbins, Probabilistic learning and reversal deficits in patients with Parkinson's disease or frontal or temporal lobe lesions: Possible adverse effects of dopaminergic medication. *Neuro*psychologia 38, 596–612 (2000).
- P. L. Remijnse, M. M. A. Nielen, A. J. L. M. van Balkom, D. C. Cath, P. van Oppen, H. B. M. Uylings, D. J. Veltman, Reduced orbitofrontal-striatal activity on a reversal learning task in obsessive-compulsive disorder. *Arch. Gen. Psychiatry* 63, 1225–1236 (2006).
- E. C. Finger, A. A. Marsh, D. G. Mitchell, M. E. Reid, C. Sims, S. Budhani, D. S. Kosson, G. Chen, K. E. Towbin, E. Leibenluft, D. S. Pine, J. R. Blair, Abnormal ventromedial prefrontal cortex function in children with psychopathic traits during reversal learning. *Arch. Gen. Psychiatry* 65, 586–594 (2008).
- V. C. Leeson, T. W. Robbins, E. Matheson, S. B. Hutton, M. A. Ron, T. R. E. Barnes, E. M. Joyce, Discrimination learning, reversal, and set-shifting in first-episode schizophrenia: Stability over six years and specific associations with medication type and disorganization syndrome. *Biol. Psychiatry* 66, 586–593 (2009).
- A. Izquierdo, J. D. Jentsch, Reversal learning as a measure of impulsive and compulsive behavior in addictions. *Psychopharmacology (Berl)* 219, 607–620 (2012).
- P. Smolen, D. A. Baxter, J. H. Byrne, Paradoxical LTP maintenance with inhibition of protein synthesis and the proteasome suggests a novel protein synthesis requirement for early LTP reversal. *J. Theor. Biol.* 457, 79–87 (2018).
- C. Dong, S. V. Bach, K. A. Haynes, A. N. Hegde, Proteasome modulates positive and negative translational regulators in long-term synaptic plasticity. *J. Neurosci.* 34, 3171–3182 (2014).
- U. Wilhelmsson, A. Pozo-Rodrigalvarez, M. Kalm, Y. de Pablo, Å. Widestrand, M. Pekna, M. Pekny, The role of GFAP and vimentin in learning and memory. *Biol. Chem.* 400, 1147–1156 (2019).
- T. J. Hausrat, M. Muhia, K. Gerrow, P. Thomas, W. Hirdes, S. Tsukita, F. F. Heisler, L. Herich, S. Dubroqua, P. Breiden, J. Feldon, J. R. Schwarz, B. K. Yee, T. G. Smart, A. Triller, M. Kneussel, Radixin regulates synaptic GABA_A receptor density and is essential for reversal learning and short-term memory. *Nat. Commun.* 6, 6872 (2015).
- L. M. DePoy, S. L. Gourley, Synaptic cytoskeletal plasticity in the prefrontal cortex following psychostimulant exposure. *Traffic* 16, 919–940 (2015).
- M. J. Wall, D. R. Collins, S. L. Chery, Z. D. Allen, E. D. Pastuzyn, A. J. George, V. D. Nikolova, S. S. Moy, B. D. Philpot, J. D. Shepherd, J. Müller, M. D. Ehlers, A. M. Mabb, S. A. L. Corrêa, The temporal dynamics of arc expression regulate cognitive flexibility. *Neuron* 98, 1124–1132.e7 (2018).
- M. K. Sung, J. M. Reitsma, M. J. Sweredoski, S. Hess, R. J. Deshaies, Ribosomal proteins produced in excess are degraded by the ubiquitin-proteasome system. *Mol. Biol. Cell* 27, 2642–2652 (2016).
- M. Hetman, L. P. Slomnicki, Ribosomal biogenesis as an emerging target of neurodevelopmental pathologies. J. Neurochem. 148, 325–347 (2019).
- D. K. Bourque, T. Hartley, S. M. Nikkel, D. Pohl, M. Tétreault, K. D. Kernohan; Care4Rare Canada Consortium, D. A. Dyment, A de novo mutation in RPL10 causes a rare X-linked ribosomopathy characterized by syndromic intellectual disability and epilepsy: A new case and review of the literature. Eur. J. Med. Genet. 61, 89–93 (2018).
- Y. J. Crow, N. Manel, Aicardi-Goutières syndrome and the type I interferonopathies. Nat. Rev. Immunol. 15, 429–440 (2015).
- J. H. Livingston, Y. J. Crow, Neurologic phenotypes associated with mutations in TREX1, RNASEH2A, RNASEH2B, RNASEH2C, SAMHD1, ADAR1, and IFIH1: Aicardi-Goutières syndrome and beyond. Neuropediatrics 47, 355–360 (2016).
- P. Araya, K. A. Waugh, K. D. Sullivan, N. G. Núñez, E. Roselli, K. P. Smith, R. E. Granrath, A. L. Rachubinski, B. E. Estrada, E. T. Butcher, R. Minter, K. D. Tuttle, T. C. Bruno, M. Maccioni, J. M. Espinosa, Trisomy 21 dysregulates T cell lineages toward an autoimmunity-prone state associated with interferon hyperactivity. *Proc. Natl. Acad. Sci. U.S.A.* 116, 24231–24241 (2019).
- K. A. Waugh, P. Araya, A. Pandey, K. R. Jordan, K. P. Smith, R. E. Granrath, S. Khanal, E. T. Butcher, B. E. Estrada, A. L. Rachubinski, J. A. McWilliams, R. Minter, T. Dimasi, K. L. Colvin, D. Baturin, A. T. Pham, M. D. Galbraith, K. W. Bartsch, M. E. Yeager, C. C. Porter, K. D. Sullivan, E. W. Hsieh, J. M. Espinosa, Mass cytometry reveals global immune

- remodeling with multi-lineage hypersensitivity to type I interferon in Down syndrome. *Cell Rep.* **29.** 1893–1908.e4 (2019).
- K. D. Sullivan, H. C. Lewis, A. A. Hill, A. Pandey, L. P. Jackson, J. M. Cabral, K. P. Smith, L. A. Liggett, E. B. Gomez, M. D. Galbraith, J. Degregori, J. M. Espinosa, Trisomy 21 consistently activates the interferon response. *eLife* 5, e16220 (2016).
- K. D. Sullivan, D. Evans, A. Pandey, T. H. Hraha, K. P. Smith, N. Markham, A. L. Rachubinski, K. Wolter-Warmerdam, F. Hickey, J. M. Espinosa, T. Blumenthal, Trisomy 21 causes changes in the circulating proteome indicative of chronic autoinflammation. *Sci. Rep.* 7, 14818 (2017)
- Y. Akwa, D. E. Hassett, M.-L. Eloranta, K. Sandberg, E. Masliah, H. Powell, J. L. Whitton, F. E. Bloom, I. L. Campbell, Transgenic expression of IFN-α in the central nervous system of mice protects against lethal neurotropic viral infection but induces inflammation and neurodegeneration. *J. Immunol.* 161, 5016–5026 (1998).
- I. L. Campbell, T. Krucker, S. Steffensen, Y. Akwa, H. C. Powell, T. Lane, D. J. Carr, L. H. Gold, S. J. Henriksen, G. R. Siggins, Structural and functional neuropathology in transgenic mice with CNS expression of IFN-α. *Brain Res.* 835, 46–61 (1999).
- D. Kavanagh, S. McGlasson, A. Jury, J. Williams, N. Scolding, C. Bellamy, C. Gunther,
 D. Ritchie, D. P. Gale, Y. S. Kanwar, R. Challis, H. Buist, J. Overell, B. Weller, O. Flossmann,
 M. Blunden, E. P. Meyer, T. Krucker, S. J. W. Evans, I. L. Campbell, A. P. Jackson, S. Chandran,
 D. P. J. Hunt, Type I interferon causes thrombotic microangiopathy by a dose-dependent toxic effect on the microvasculature. *Blood* 128, 2824–2833 (2016).
- T. Goldmann, N. Zeller, J. Raasch, K. Kierdorf, K. Frenzel, L. Ketscher, A. Basters,
 O. Staszewski, S. M. Brendecke, A. Spiess, T. L. Tay, C. Kreutz, J. Timmer, G. M. Mancini,
 T. Blank, G. Fritz, K. Biber, R. Lang, D. Malo, D. Merkler, M. Heikenwälder, K. Knobeloch,
 M. Prinz, USP18 lack in microglia causes destructive interferonopathy of the mouse brain.
 EMBO J. 34. 1612–1629 (2015).
- J. Eggenberger, D. Blanco-Melo, M. Panis, K. J. Brennand, B. R. ten Oever, Type I interferon response impairs differentiation potential of pluripotent stem cells. *Proc. Natl. Acad. Sci.* U.S.A. 116, 1384–1393 (2019).
- Q. Yu, Y. V. Katlinskaya, C. J. Carbone, B. Zhao, K. V. Katlinski, H. Zheng, M. Guha, N. Li,
 Q. Chen, T. Yang, C. J. Lengner, R. A. Greenberg, F. B. Johnson, S. Y. Fuchs, DNA-Damage-Induced Type I Interferon Promotes Senescence and Inhibits Stem Cell Function. *Cell Rep.* 11, 785–797 (2015).
- 87. K. Zhu, K. Dunner Jr., D. J. McConkey, Proteasome inhibitors activate autophagy as a cytoprotective response in human prostate cancer cells. *Oncogene* **29**, 451–462 (2010).
- M. Studencka-Turski, G. Çetin, H. Junker, F. Ebstein, E. Krüger, Molecular Insight Into the IRE1α-Mediated Type I Interferon Response Induced by Proteasome Impairment in Myeloid Cells of the Brain. Front. Immunol. 10, 2900 (2019).
- M. Khacho, R. Harris, R. S. Slack, Mitochondria as central regulators of neural stem cell fate and cognitive function. *Nat. Rev. Neurosci.* 20, 34–48 (2019).
- K. Yang, R. Huang, H. Fujihira, T. Suzuki, N. Yan, N-glycanase NGLY1 regulates mitochondrial homeostasis and inflammation through NRF1. J. Exp. Med. 215, 2600–2616 (2018).
- A. J. Sadler, B. R. G. Williams, Structure and function of the protein kinase R. Curr. Top. Microbiol. Immunol. 316, 253–292 (2007).
- D. W. Reid, Q. Chen, A. S. L. Tay, S. Shenolikar, C. V. Nicchitta, The unfolded protein response triggers selective mRNA release from the endoplasmic reticulum. *Cell* 158, 1362–1374 (2014).
- E. Meurs, K. Chong, J. Galabru, N. S. B. Thomas, I. M. Kerr, B. R. G. Williams,
 A. G. Hovanessian, Molecular cloning and characterization of the human double-stranded RNA-activated protein kinase induced by interferon. *Cell.* 62, 379–390 (1990).
- M. Benkirane, C. Neuveut, R. F. Chun, S. M. Smith, C. E. Samuel, A. Gatignol, K. T. Jeang, Oncogenic potential of TAR RNA binding protein TRBP and its regulatory interaction with RNA-dependent protein kinase PKR. EMBO J. 16, 611–624 (1997).
- R. C. Patel, G. C. Sen, PACT, a protein activator of the interferon-induced protein kinase, PKR. EMBO J. 17, 4379–4390 (1998).
- N. Siwecka, W. Rozpędek-Kamińska, A. Wawrzynkiewicz, D. Pytel, J. A. Diehl, I. Majsterek, The structure, activation and signaling of IRE1 and its role in determining cell fate. *Biomedicine* 9, 156 (2021).
- M. A. Deture, D. W. Dickson, The neuropathological diagnosis of Alzheimer's disease. Mol. Neurodegener. 14, 32 (2019).
- S. Gal-Ben-Ari, I. Barrera, M. Ehrlich, K. Rosenblum, PKR: A kinase to remember. Front. Mol. Neurosci. 11, 480 (2019).
- J. A. Marchal, G. J. Lopez, M. Peran, A. Comino, J. R. Delgado, J. A. García-García, V. Conde, F. M. Aranda, C. Rivas, M. Esteban, M. A. García, The impact of PKR activation: From neurodegeneration to cancer. FASEB J. 28. 1965–1974 (2014).
- E. Chukwurah, K. T. Farabaugh, B. J. Guan, P. Ramakrishnan, M. Hatzoglou, A tale of two proteins: PACT and PKR and their roles in inflammation. FEBS J. 288, 6365–6391 (2021).

SCIENCE TRANSLATIONAL MEDICINE | RESEARCH ARTICLE

- L. Muzio, A. Viotti, G. Martino, Microglia in Neuroinflammation and Neurodegeneration: From Understanding to Therapy. Front. Neurosci. 15, 742065 (2021).
- M. M. Ahmed, N. R. Johnson, T. D. Boyd, C. Coughlan, H. J. Chial, H. Potter, Innate Immune System Activation and Neuroinflammation in Down Syndrome and Neurodegeneration: Therapeutic Targets or Partners? Front. Aging Neurosci. 13, 718426 (2021).
- N. Sobreira, F. Schiettecatte, D. Valle, A. Hamosh, GeneMatcher: A matching tool for connecting investigators with an interest in the same gene. *Hum. Mutat.* 36, 928–930 (2015).
- K. J. Karczewski, L. C. Francioli, G. Tiao, B. B. Cummings, J. Alföldi, Q. Wang, R. L. Collins, K. M. Laricchia, A. Ganna, D. P. Birnbaum, L. D. Gauthier, H. Brand, M. Solomonson, N. A. Watts, D. Rhodes, M. Singer-Berk, E. M. England, E. G. Seaby, J. A. Kosmicki, R. K. Walters, K. Tashman, Y. Farjoun, E. Banks, T. Poterba, A. Wang, C. Seed, N. Whiffin, J. X. Chong, K. E. Samocha, E. Pierce-Hoffman, Z. Zappala, A. H. O'Donnell-Luria, E. V. Minikel, B. Weisburd, M. Lek, J. S. Ware, C. Vittal, I. M. Armean, L. Bergelson, K. Cibulskis, K. M. Connolly, M. Covarrubias, S. Donnelly, S. Ferriera, S. Gabriel, J. Gentry, N. Gupta, T. Jeandet, D. Kaplan, C. Llanwarne, R. Munshi, S. Novod, N. Petrillo, D. Roazen, V. Ruano-Rubio, A. Saltzman, M. Schleicher, J. Soto, K. Tibbetts, C. Tolonen, G. Wade, M. E. Talkowski; Genome Aggregation Database Consortium, B. M. Neale, M. J. Daly, D. G. MacArthur, The mutational constraint spectrum quantified from variation in 141,456 humans. Nature 581, 434–443 (2020).
- 105. D. Taliun, D. N. Harris, M. D. Kessler, J. Carlson, Z. A. Szpiech, R. Torres, S. A. G. Taliun, A. Corvelo, S. M. Gogarten, H. M. Kang, A. N. Pitsillides, J. LeFaive, S.-b. Lee, X. Tian, B. L. Browning, S. Das, A. K. Emde, W. E. Clarke, D. P. Loesch, A. C. Shetty, T. W. Blackwell, A. V. Smith, O. Wong, X. Liu, M. P. Conomos, D. M. Bobo, F. Aguet, C. Albert, A. Alonso, K. G. Ardlie, D. E. Arking, S. Aslibekyan, P. L. Auer, J. Barnard, R. G. Barr, L. Barwick, L. C. Becker, R. L. Beer, E. J. Benjamin, L. F. Bielak, J. Blangero, M. Boehnke, D. W. Bowden, J. A. Brody, E. G. Burchard, B. E. Cade, J. F. Casella, B. Chalazan, D. I. Chasman, Y. D. I. Chen, M. H. Cho, S. H. Choi, M. K. Chung, C. B. Clish, A. Correa, J. E. Curran, B. Custer, D. Darbar, M. Dava, M. de Andrade, D. L. DeMeo, S. K. Dutcher, P. T. Ellinor, L. S. Emery, C. Eng. D. Fatkin, T. Fingerlin, L. Forer, M. Fornage, N. Franceschini, C. Fuchsberger, S. M. Fullerton, S. Germer, M. T. Gladwin, D. J. Gottlieb, X. Guo, M. E. Hall, J. He, N. L. Heard-Costa, S. R. Heckbert, M. R. Irvin, J. M. Johnsen, A. D. Johnson, R. Kaplan, S. L. R. Kardia, T. Kelly, S. Kelly, E. E. Kenny, D. P. Kiel, R. Klemmer, B. A. Konkle, C. Kooperberg, A. Köttgen, L. A. Lange, J. Lasky-Su, D. Levy, X. Lin, K. H. Lin, C. Liu, R. J. F. Loos, L. Garman, R. Gerszten, S. A. Lubitz, K. L. Lunetta, A. C. Y. Mak, A. Manichaikul, A. K. Manning, R. A. Mathias, D. D. McManus, S. T. McGarvey, J. B. Meigs, D. A. Meyers, J. L. Mikulla, M. A. Minear, B. D. Mitchell, S. Mohanty, M. E. Montasser, C. Montgomery, A. C. Morrison, J. M. Murabito, A. Natale, P. Natarajan, S. C. Nelson, K. E. North, J. R. O'Connell, N. D. Palmer, N. Pankratz, G. M. Peloso, P. A. Peyser, J. Pleiness, W. S. Post, B. M. Psaty, D. C. Rao, S. Redline, A. P. Reiner, D. Roden, J. I. Rotter, I. Ruczinski, C. Sarnowski, S. Schoenherr, D. A. Schwartz, J. S. Seo, S. Seshadri, V. A. Sheehan, W. H. Sheu, M. B. Shoemaker, N. L. Smith, J. A. Smith, N. Sotoodehnia, A. M. Stilp, W. Tang, K. D. Taylor, M. Telen, T. A. Thornton, R. P. Tracy, D. J. van den Berg, R. S. Vasan, K. A. Viaud-Martinez, S. Vrieze, D. E. Weeks, B. S. Weir, S. T. Weiss, L. C. Weng, C. J. Willer, Y. Zhang, X. Zhao, D. K. Arnett, A. E. Ashley-Koch, K. C. Barnes, E. Boerwinkle, S. Gabriel, R. Gibbs, K. M. Rice, S. S. Rich, E. K. Silverman, P. Qasba, W. Gan; NHLBI Trans-Omics for Precision Medicine (TOPMed) Consortium, G. J. Papanicolaou, D. A. Nickerson, S. R. Browning, M. C. Zody, S. Zöllner, J. G. Wilson, L. A. Cupples, C. C. Laurie, C. E. Jaquish, R. D. Hernandez, T. D. O'Connor, G. R. Abecasis, Sequencing of 53,831 diverse genomes from the NHLBI TOPMed Program. Nature 590, 290-299 (2021).
- J. F. Fonteneau, M. Larsson, S. Somersan, C. Sanders, C. Münz, W. W. Kwok, N. Bhardwaj, F. Jotereau, Generation of high quantities of viral and tumor-specific human CD4+ and CD8+T-cell clones using peptide pulsed mature dendritic cells. J. Immunol. Methods 258, 111–126 (2001).
- F. V. Bolduc, K. Bell, H. Cox, K. S. Broadie, T. Tully, Excess protein synthesis in Drosophila Fragile X mutants impairs long-term memory. *Nat. Neurosci.* 11, 1143–1145 (2008).
- L. M. Palma Medina, A. K. Becker, S. Michalik, H. Yedavally, E. J. M. Raineri, P. Hildebrandt, M. G. Salazar, K. Surmann, H. Pförtner, S. A. Mekonnen, A. Salvati, L. Kaderali, J. M. Van Dijl, U. Völker, Metabolic Cross-talk between Human Bronchial Epithelial Cells and Internalized Staphylococcus aureus as a Driver for Infection. *Mol. Cell. Proteomics* 18, 892–908 (2019).
- T. Suomi, L. L. Elo, Enhanced differential expression statistics for data-independent acquisition proteomics. Sci. Rep. 7, 5869 (2017).
- B. Phipson, S. Lee, I. J. Majewski, W. S. Alexander, G. K. Smyth, ROBUST HYPERPARAMETER ESTIMATION PROTECTS AGAINST HYPERVARIABLE GENES AND IMPROVES POWER TO DETECT DIFFERENTIAL EXPRESSION. Ann. Appl. Stat. 10, 946–963 (2016).
- Y. Perez-Riverol, J. Bai, C. Bandla, D. García-Seisdedos, S. Hewapathirana,
 Kamatchinathan, D. J. Kundu, A. Prakash, A. Frericks-Zipper, M. Eisenacher, M. Walzer,

- S. Wang, A. Brazma, J. A. Vizcaíno, The PRIDE database resources in 2022: A hub for mass spectrometry-based proteomics evidences. *Nucleic Acids Res.* **50**, D543–D552 (2022).
- 112. A. Knaus, J. T. Pantel, M. Pendziwiat, N. Hajjir, M. Zhao, T. C. Hsieh, M. Schubach, Y. Gurovich, N. Fleischer, M. Jäger, S. Köhler, H. Muhle, C. Korff, R. S. Møller, A. Bayat, P. Calvas, N. Chassaing, H. Warren, S. Skinner, R. Louie, C. Evers, M. Bohn, H. J. Christen, M. van den Born, E. Obersztyn, A. Charzewska, M. Endziniene, F. Kortüm, N. Brown, P. N. Robinson, H. J. Schelhaas, Y. Weber, I. Helbig, S. Mundlos, D. Horn, P. M. Krawitz, Characterization of glycosylphosphatidylinositol biosynthesis defects by clinical features, flow cytometry, and automated image analysis. Genome Med. 10, 3 (2018).
- 113. F. Marbach, C. F. Rustad, A. Riess, D. Đukić, T. C. Hsieh, I. Jobani, T. Prescott, A. Bevot, F. Erger, G. Houge, M. Redfors, J. Altmueller, T. Stokowy, C. Gilissen, C. Kubisch, E. Scarano, L. Mazzanti, T. Fiskerstrand, P. M. Krawitz, D. Lessel, C. Netzer, The Discovery of a LEMD2-Associated Nuclear Envelopathy with Early Progeroid Appearance Suggests Advanced Applications for Al-Driven Facial Phenotyping. Am. J. Hum. Genet. 104, 749–757 (2019).
- M. Oti, M. A. Huynen, H. G. Brunner, Phenome connections. Trends Genet. 24, 103–106 (2008).
- Y. Gurovich, Y. Hanani, O. Bar, G. Nadav, N. Fleischer, D. Gelbman, L. Basel-Salmon,
 P. M. Krawitz, S. B. Kamphausen, M. Zenker, L. M. Bird, K. W. Gripp, Identifying facial phenotypes of genetic disorders using deep learning. *Nat. Med.* 25, 60–64 (2019).
- K. Goslin, G. Banker, Rapid changes in the distribution of GAP-43 correlate with the expression of neuronal polarity during normal development and under experimental conditions. J. Cell Biol. 110, 1319–1331 (1990).

Acknowledgments: The sequencing for patient #3 was performed under the Care4Rare Canada Consortium funded by Genome Canada and the Ontario Genomics Institute (OGI-147), the Canadian Institutes of Health Research, Ontario Research Fund, Genome Alberta, Genome British Columbia, Genome Quebec, and Children's Hospital of Eastern Ontario Foundation. The DDD study presents independent research commissioned by the Health Innovation Challenge Fund (grant number HICF-1009-003). This study makes use of DECIPHER (www. deciphergenomics.org), which is funded by the Wellcome Trust. We are grateful to R. Beyer and A. Brandenburg for excellent technical assistance. Funding: This work was supported by the German Research Foundation grant SFBTR167, RGT2719-PRO project B4 to E.K., E-Rare project GENOMIT (Austrian Science Fund FWF, I4695-B) to J.A.M., U.S. National Institutes of Health (NIH) grant (R01MH101221), and a grant from the Simons Foundation (SFARI #608045) to E.E.E. E.E.E. is an investigator of the Howard Hughes Medical Institute. This work was also supported, in part, by "the Fundamental Research Funds for the Central Universities" starting fund (BMU2022RCZX038) to T.W. Author contributions: Patient enrollment was supervised by S.K. Acquisition of genomic and clinical data was supervised by S.K., T.W., E.E.E., and S.B. The behavioral studies were designed, conducted, and analyzed by C.R. and F.B. The structural modeling studies were carried out by V.M. and P.W.H. Facial image analysis of patients was made by T.-C.H. and P.K. The in vivo neuronal morphology assays were designed, performed, and analyzed by G.M.v.W., C.d.K., S.M.W.T., and Y.E. The functional in vitro experiments on SHSY5Y cells and T cells were performed by F.E., J.J.P., R.G., T. Besnard, V.V., and W.D. and analyzed by F.E. and E.K. Proteomic investigations were conducted by E.H. and U.V. and analyzed by E.H., U.V., M.-P.S.-B., and A.D. Gene expression analysis by NanoString was made by M.S.T., F.E., and E.K. T. Brunet, D.B., C.F., R.H.v.J., L.A., B.C., C.M., M.C.J.J., F.S.C., M.-J.H.v.d.B., J.A.W., DIW SY VH JAB NZ BB BK A-CG ZP MT KB AS AFB JM RW KA JH MTC M.O., P.G.W., F.F., S.M., Y.T., A.A., R.H., Y.G., S.R., G.B., R.G.F., J.A.M., M.P., F.L., T.K., A.K., and B.I. made important conceptual contributions and provided critical material and/or patients' clinical data to carry out the research. F.E and S.K. drafted the manuscript. F.E, S.K., E.K., and S.B. edited and revised the manuscript. All authors approved the final version of the manuscript. Competing interests: The authors declare that they have no competing interests. Data and materials availability: All data associated with this study are present in the paper or the Supplementary Materials. The mass spectrometry proteomics were deposited to the ProteomeXchange Consortium via the PRIDE partner repository with the dataset identifier PXD041182. Datasets from transcriptomics analysis (NanoString) were deposited to the GEO repository under accession number GSE228675. Plasmids generated in this study can be provided by E.K. under a Universitaetsmedizin Greifswald material transfer agreement. Human cells derived from patients #13, #17, #18, and #21 are stored in the University Medicine Greifswald Biobank. Availability of patient's samples is restricted depending on patient's consent for follow-up

Submitted 28 January 2022 Accepted 10 May 2023 Published 31 May 2023 10.1126/scitranslmed.abo3189

analysis.